A European aerosol phenomenology-6: Scattering properties of atmospheric aerosol particles from 28 ACTRIS sites

Marco Pandolfi[1], Lucas Alados-Arboledas[2], Andrés Alastuey[1], Marcos Andrade[3], Christo Angelov[4], Begoña Artiñano[5], John Backman[6,7], Urs Baltensperger[8], Paolo Bonasoni[9], Nicolas Bukowiecki[8], Martine Collaud Coen[10], Sébastien Conil[11], Esther Coz[5], Vincent Crenn[12,13], Vadimas Dudoitis[14], Marina Ealo[1], Kostas Eleftheriadis[15], Olivier Favez[16], Prodromos Fetfatzis[15], Markus Fiebig[17], Harald Flentje[18], Patrick Ginot[19], Martin Gysel[8], Bas Henzing[20], Andras Hoffer[21], Adela Holubova Smejkalova[22,23], Ivo Kalapov[4], Nikos Kalivitis[24,25], Giorgos Kouvarakis[24], Adam Kristensson[26], Markku Kulmala[6], Heikki Lihavainen[7], Chris Lunder[17], Krista Luoma[6], Hassan Lyamani[2], Angela Marinoni[9], Nikos Mihalopoulos[24,25], Marcel Moerman[20], José Nicolas[27], Colin O'Dowd[28], Tuukka Petäjä[6], Jean-Eudes Petit[12,16], Jean Marc Pichon[27], Nina Prokopciuk[14], Jean-Philippe Putaud[29], Sergio Rodríguez[30], Jean Sciare[12,a], Karine Sellegri[27], Erik Swietlicki[26], Gloria Titos[2], Thomas Tuch[31], Peter Tunved[32], Vidmantas Ulevicius[14], Aditya Vaishya[28,33], Milan Vana[22,23], Aki Virkkula[6], Stergios Vratolis[15], Ernest Weingartner[8,b], Alfred Wiedensohler[31], and Paolo Laj[6,9,19]

[1] Institute of Environmental Assessment and Water Research, c/ Jordi-Girona 18-26, 08034, Barcelona, Spain
[2] Andalusian Institute for Earth System Research, IISTA-CEAMA, University of Granada, Granada 18006, Spain
[3] Atmospheric Physics Laboratory, ALP, UMSA, Campus Cota Cota calle 27, Endifico FCPN piso 3, La Paz, Bolivia
[4] Institute for Nuclear Research and Nuclear Energy by the Bulgarian Academy of Sciences, 72 Tsarigradsko Chaussee Blvd, 1784-Sofia, Bulgaria
[5] Centro de Investigaciones Energéticas, Medioambientales y Tecnológicas, CIEMAT, Unidad Asociada en Contaminación Atmosférica, CIEMAT-CSIC, Avda. Complutense, 40, 28040 Madrid
[6] University of Helsinki, UHEL, Division of Atmospheric Sciences, PO BOX 64, FI-00014, Helsinki, Finland
[7] Finnish Meteorological Institute, FMI, Erik Palmenin aukio 1, FI-00560, Helsinki, Finland
[8] Paul Scherrer Institut, PSI, Laboratory of Atmospheric Chemistry (LAC), OFLB, , 5232, Villigen PSI, Switzerland
[9] Institute of Atmospheric Sciences and Climate, ISAC, Via P. Gobetti 101, I-40129, Bologna, Italy
[10] Federal Office of Meteorology and Climatology, MeteoSwiss, Chemin de l'aérologie, 1530 Payerne, Switzerland
[11] ANDRA – DRD – Observation Surveillance, Observatoire Pérenne de l'Environnement, Bure, France
[12] LSCE-Orme point courrier 129 CEA-Orme des Merisiers, 91191 Gif-sur-Yvette, France
[13] ADDAIR, BP 70207 - 189, rue Audemars, 78530, Buc, France
[14] SRI Center for Physical Sciences and Technology, CPST, Sauletekio ave. 3, LT-10257, Vilnius, Lithuania
[15] Institute of Nuclear & Radiological Science & Technology, Energy & Safety, N.C.S.R. "Demokritos", Athens, 15341, Greece
[16] Institut National de l'Environnement Industriel et des Risques, Verneuil en Halatte, 60550, France
[17] Norwegian Institute for Air Research, Atmosphere and Climate Department, NILU, Instituttveien 18, , 2007, Kjeller, Norway
[18] Deutscher Wetterdienst, Met. Obs. Hohenpeissenberg, DE-82383 Hohenpeissenberg, Germany
[19] Univ. Grenoble-Alpes, CNRS, IRD, INPG, IGE F-38000 Grenoble, France
[20] TNO B&O, Princetonlaan 6, 3584TA, The Hague, The Netherlands
[21] MTA-PE Air Chemistry Research Group, Veszprém, P.O. Box 158, H-8201, Hungary
[22] Global Change Research Institute AS CR, Belidla 4a, 603 00, Brno, Czech Republic
[23] Czech Hydrometeorological Institute, Na Sabatce 17 , 143 06, Praha, Czech Republic.
[24] Environmental Chemical Processes Laboratory, Dept. of Chemistry, Univ. of Crete, Heraklion, 71003, Greece
[25] Institute for Environmental Research & Sustainable Development, National Observatory of Athens (NOA), I. Metaxa & Vas. Pavlou, 15236 Palea Penteli, Greece
[26] Lund University, Department of Physics, P. O. Box 118, SE-22100, Lund, Sweden
[27] CNRS-LaMP Université Blaise Pascal 4, Avenue Blaise Pascal 63178 Aubiere Cedex, France

[28] School of Physics and Centre for Climate & Air Pollution Studies, Ryan Institute, National University of Ireland Galway, University Road, Galway, Ireland
[29] EC Joint Research Centre, EC-JRC-IES, Institute for Environment and Sustainability, Via Enrico Fermi 2749, 21027, Ispra, Italy
[30] Agencia Estatal de Meteorologia, AEMET, Izaña Atmospheric Research Center, La Marina 20, E-38071, Santa Cruz de Tenerife, Spain
[31] Leibniz Institute for Tropospheric Research, (TROPOS), Permoserstraße 15, 04318, Leipzig, Germany
[32] Department of Environmental Science and Analytical Chemistry (ACES) and the Bolin Centre for Climate Research, Stockholm University, SE-106 91 Stockholm, Sweden
[33] Space Physics Laboratory, Vikram Sarabhai Space Centre, ISRO, Thiruvananthapuram – 695022, India.

[a] now at: EEWRC, The Cyprus Institute, Nicosia, Cyprus
[b] now at: Institute for Aerosol and Sensor Technology, University of Applied Sciences (FHNW), Windisch, Switzerland

1   **Abstract**
2
3   This paper presents the light scattering properties of atmospheric aerosol particles measured over
4   the past decade at 28 ACTRIS observatories which are located mainly in Europe. The data include
5   particle light scattering (σ_{sp}) and hemispheric backscattering (σ_{bsp}) coefficients, scattering Ångström
6   exponent (SAE), backscatter fraction (BF) and asymmetry parameter (g). An increasing gradient of
7   σ_{sp} is observed when moving from remote environments (Arctic/mountain) to regional and to urban
8   environments. At regional level in Europe, σ_{sp} also increases when moving from Nordic and Baltic
9   countries and Western Europe to Central/Eastern Europe whereas no clear spatial gradient is
10   observed for other station environments. The SAE does not show a clear gradient as a function of
11   the placement of the station. However, a West to East increasing gradient is observed for both
12   regional and mountain placements suggesting a lower fraction of fine-mode particle in
13   Western/Southwestern Europe compared to Central and Eastern Europe where the fine-mode
14   particles dominate the scattering. The g does not show any clear gradient by station placement or
15   geographical location reflecting the complex relationship of this parameter with the aerosol
16   particles physical properties. Both the station placement and the geographical location are
17   important factors affecting the intra-annual variability. At mountain sites, higher σ_{sp} and SAE values
18   are measured in the summer due to the enhanced boundary layer influence and/or new particles
19   formation episodes. Conversely, the lower horizontal and vertical dispersion during winter leads to
20   higher σ_{sp} values at all low altitude sites in Central and Eastern Europe compared to summer.
21   These sites also show SAE maxima in the summer (with corresponding g minima). At all sites, both
22   SAE and g show a strong variation with aerosol particle loading. The lowest values of g are always
23   observed together with low σ_{sp} values, indicating a larger contribution from particles in the smaller
24   accumulation mode. During periods of high σ_{sp} values, the variation of g is less pronounced
25   whereas the SAE increases or decreases, suggesting changes mostly in the coarse aerosol
26   particle mode rather than in the fine mode. Statistically significant decreasing trends of σ_{sp} are
27   observed at 5 out of the 13 stations included in the trend analyses. The total reductions of σ_{sp} are
28   consistent with those reported for $PM_{2.5}$ and PM_{10} mass concentrations over similar periods across
29   Europe.

31   **1. Introduction**

32   Atmospheric aerosol particles are recognized as an important atmospheric constituent which have
33   demonstrated effects on climate and health. The radiative forcing of aerosol particles, estimated as
34   −0.9 [−1.9 to −0.1] W/m^2 (IPCC, 2014), has two competing components: a cooling effect from most
35   particle types and a partially offsetting warming contribution from black carbon (BC) particle light
36   absorption of solar radiation. The aerosol cooling is the dominant effect; thus aerosol particles
37   counteract a substantial portion of the warming effect from well-mixed greenhouse gases (GHGs).
38   This process is driven by the scattering properties of most aerosol particle types (e.g. secondary

sulphate and nitrate particles, mineral and organic matter), which reduce the amount of solar radiation reaching the Earth's surface, instead reflecting it back into space thus modifying the Earth's radiative balance.

However, the high temporal and spatial variability of atmospheric aerosol particles, due to the wide variety of aerosol sources and sinks, together with their short and variable lifetimes (hours to weeks in the planetary boundary layer) and spatial non-uniformity, constitute the largest uncertainties in the estimation of the total radiative forcing. Reducing these uncertainties is mandatory in view of the global warming the planet has experienced over the past 50 years. In fact, there is evidence suggesting that the observed (and projected) decrease in emissions of anthropogenic aerosol particles in response to air quality policies will eventually exert a positive aerosol effective radiative forcing at the top of the atmosphere (Rotstayn et al., 2013). Thus, current emission controls could both enhance climate warming while improving air quality (e.g. Stohl et al., 2015).

The measurements of aerosol particle optical properties, such as light scattering and absorption, together with measurements of their physical and chemical properties, are fundamental in order to better understand the current trade-off between the impacts of aerosols on environmental health and the Earth's climate. In recent decades, several international projects have provided important information on atmospheric particle properties worldwide. Near-surface in situ observations of aerosol particle properties are being made worldwide under the GAW/WMO (Global Atmosphere Watch; http://www.wmo.int/pages/prog/arep/gaw/gaw_home_en.html) program and are complemented with policy-oriented programs such as IMPROVE (Interagency Monitoring of Protected Visual Environments; http://vista.cira.colostate.edu/Improve/) in the United States and EMEP (European Monitoring and Evaluation Programme; http://www.emep.int/) in Europe. Additional information specifically targeting advanced aerosol particle properties have been obtained in Europe using information from the European research infrastructure ACTRIS (Aerosols, Clouds, and Trace gases Research InfraStructure; http://www.actris.eu) and from short-term RTD (Research and Technological Development) projects such as EUCAARI (European Integrated Project on Aerosol Cloud Climate and Air Quality Interactions; http://www.cas.manchester.ac.uk/resprojects/eucaari/).

The implementation of the GAW program in Europe is performed under ACTRIS in regard to the advanced observation of aerosol particle properties. ACTRIS provides harmonized measurements of different (physical, chemical and optical) aerosol properties in a systematic way at major observation sites across Europe. More than 60 measuring sites worldwide are currently providing ground-based in situ aerosol particle light scattering measurements (EBAS database; www. http://ebas.nilu.no/) and this number has increased substantially in the last decade. However, EBAS also includes data from the IMPROVE network nephelometers, which latter are

operated at ambient conditions with no size cut, as a result of which these IMPROVE data are not directly comparable to the ACTRIS dataset discussed in this investigation.

The objective of this work is to integrate the total aerosol light scattering coefficient (σ_{sp}) and hemispheric backscattering coefficient (σ_{bsp}) measurements performed over several years at the ground based in situ ACTRIS stations. A total of 28 stations (26 European + 2 non-European) are included in order to document the variability in near-surface aerosol particle light scattering across the ACTRIS network. Moreover, at some of the ACTRIS stations more than 10 years of σ_{sp} data are available, allowing us to perform trend analyses. The study of the trend of σ_{sp} is important given that a decreasing or increasing trend of σ_{sp} over time would be indicative of the effectiveness of the air quality control measures. In fact, many studies have shown that the concentrations of particulate matter (PM), and other air pollutants such as sulphur dioxide (SO_2) and carbon monoxide (CO), have clearly decreased during the last 20 years in many European countries (Barmpadimos et al., 2012; Cusack et al., 2012; EEA, 2013; Querol et al., 2014; Guerreiro et al., 2014; Pandolfi et al., 2016, Tørseth et al., 2012, among others).

Previous studies presenting multi-site ground-based in situ aerosol particle optical measurements were, for example, performed by Delene and Ogren (2002), Sherman et al. (2015), Collaud Coen et al. (2013) and Andrews et al. (2011). Delene and Ogren (2002) and Sherman et al. (2015) reported on the variability of aerosol particle optical properties at four North American surface monitoring sites. Collaud Coen et al. (2013) presented long term (>8-9 years) aerosol particle light scattering and absorption measurements performed at 24 regional/remote observatories located mostly in the United States (although 5 are located in Europe). Andrews et al. (2011) reported aerosol particle optical measurements performed at 12 mountain top observatories (4 of which are located in Europe, 5 in the United States and Canada and 3 in Asia).

Our work is focused mainly on European observatories and is aimed at presenting a representative phenomenology of aerosol particle light scattering coefficients measurements at ACTRIS stations. Thanks to the establishment of European monitoring networks and/or research projects, five papers relating to aerosol phenomenology have been published in Europe: Van Dingenen et al. (2004) and Putaud et al. (2004), respectively, on the physical and chemical characteristics of particulate matter (PM) at the kerbside, urban, rural and background sites in Europe; Putaud et al. (2010) on the physical and chemical characteristics of PM measured at 60 sites across Europe; Cavalli et al. (2016) on the harmonized concentrations of carbonaceous aerosols at ten regional background sites in Europe; and Zanatta et al. (2016) presenting a climatology of BC optical properties at nine European regional background sites. The importance of these studies and of the present work rests on the premise that a reliable assessment of the physical, chemical and optical properties of aerosol particles at a European scale is of crucial importance for an accurate estimation of the radiative forcing of atmospheric aerosols. This work is the first European phenomenology study dedicated to the light scattering properties of aerosol

particles measured in situ at near-surface ground-based observatories. Moreover, the trend analyses presented can be used to evaluate how the European mitigation strategies adopted to improve air quality have impacted aerosol particle optical properties.

2. Experimental

2.1 Atmospheric Observatories

Figure 1 shows the location of the observatories which are grouped according to their geographical locations, a grouping employed in other European phenomenology studies (e.g. Putaud et al., 2010). Observatory information (country, code, coordinates, altitude, geographical location, among others) and measurement periods are summarized in Table 1. The observatories are also divided into five different categories depending on their placement within each geographical sector. Arctic: includes stations located in the Arctic/sub-Arctic region; mountain: includes those observatories located at more than 985 m above sea level (the lowest altitude among the mountain observatories included here); coastal: includes observatories located close to the coast (<1-4 km); regional/rural: includes those observatories that are representative of large regional areas; urban/sub-urban: includes observatories located in a background of an urban or suburban area. Two non-European stations are also included; one Antarctic site and one mountain site in Bolivia. Given that this work mainly focuses on European ACTRIS observatories, the results from these two non-European stations are reported in the Supporting Information.

The altitude of the mountain stations considered here range between 985 m at HPB and 5240 m at CHC (cf. Table 1). Some of the mountain stations included in this investigation have already been included in the work of Andrews et al. (2011), namely IZO, JFJ, CMN, and BEO. Moreover, the FKL, HPB, JFJ, MHD and PAL stations have been included in the study by Collaud Coen et al. (2013). Both studies presented in situ aerosol particle optical measurements taken at these stations. The main results of these previous investigations are summarized in the results section.

2.2 Scattering measurements

2.2.1 Instruments

The measurements of σ_{sp} and σ_{bsp} included in this study were obtained from TSI and Ecotech integrating nephelometers (Table 1). These optical instruments measure the amount of light scattered by particles in the visible spectrum and provide σ_{sp} and σ_{bsp} coefficients of the sampled aerosols. The most common nephelometers in the ACTRIS program are the TSI3563 and the Ecotech AURORA3000 nephelometers, both of which provide both σ_{sp} and σ_{bsp}. Model TSI3563 measures σ_{sp} and σ_{bsp} at 450, 550 and 700 nm whereas the Ecotech AURORA3000 measures at

450, 525 and 635 nm. Other models used are the M9003 from Ecotech (SIR and CMN) and the RR (Radiance Research) nephelometer model M903 (FKL) measuring σ_{sp} at 520 nm and 532 nm, respectively. Due to the non-homogeneity of the angular distribution of light intensity of model M9003 (cf. Müller et al., 2009), the light source was changed at SIR in 2013 with the AURORA3000 light source and at CMN in 2009 with an opal glass light source. After the change of the light sources, both nephelometers were examined at the World Calibration Center for Aerosol Physical properties in Leipzig and both performed very well (personal communication from CMN and SIR data providers). The detailed description of the main characteristics and the working principle of the integrating nephelometers can be found e.g. in Müller et al. (2011) for the Ecotech AURORA3000 and in Anderson and Ogren (1998) for the model TSI 3563.

Recommended quality assurance procedures during on-site operation, as described in GAW (WMO-GAW Report, 2016), help to ensure the quality and comparability of the data. The nephelometers included in this investigation are regularly calibrated using span gas and are zero adjusted using particle-free air. Additionally, most of the integrating nephelometers employed in ACTRIS have undergone a schedule of performance checks at the World Calibration Center for Aerosol Physics of ACTRIS/GAW.

2.2.2 Data treatment

Data used in this investigation include hourly averaged Level 2 aerosol particle scattering data downloaded from the ACTRIS/EBAS Data Centre web portals (www.actris.nilu.no; www.ebas.nilu.no; last downloads August 2017). The σ_{sp} and σ_{bsp} data reported to EBAS and used in this work are referenced to standard T (273.15 ºC) and P (1013 hPa) conditions. Data consistency is critical when comparing many years' worth of data from different stations. In this work, the Level 2 scattering data were further reviewed in order to ensure a high quality of the data presented. There are however station-to-station differences (e.g. sizecut, RH control, wavelength, data processing, etc.) which are addressed in the sections below.

2.2.2.1 Truncation correction

Data from the integrating nephelometers used here are corrected for non-ideal illumination of the light source (deviation from a Lambertian distribution of light) and for truncation of the sensing volumes in the near-forward (around 0-10º) and near-backward (around 170-180º) directions (Müller et al., 2009 and Anderson and Ogren, 1998). Correction schemes have been provided by Müller et al. (2009; 2011) for the RR M903 and Ecotech models M9003 and AURORA3000, and by Anderson and Ogren (1998) for the TSI3563. These schemes consist of a simple linear correction based on the scattering Ångström exponent (SAE) determined from the raw nephelometer data to take account of the size-distribution-dependent truncation error. It has been demonstrated that

these simple correction schemes are accurate for a wide range of atmospheric aerosols and that the uncertainties in the corrections are not expected to be larger than 2% for an aerosol particle population with a single scattering albedos (SSA) greater than 0.8 (Bond et al., 2009).

The majority of the σ_{sp} data in the EBAS database are corrected for non-ideal illumination and for truncation by the data providers. Exceptions are the scattering data submitted for KOS, MHD, PLA, CMN, FKL and SIR. Scattering data from KOS, MHD and PLA were corrected in this work using the correction scheme provided by Anderson and Ogren (1998) (cf. Table S1 of the Supporting Material). The σ_{sp} data collected at CMN, FKL and SIR are not corrected because the nephelometers deployed at these three stations provide scattering only at one wavelength, thus preventing the estimation of the SAE. Given that the nephelometer correction factors vary as a function of SAE, the assumption of a constant correction factor to correct the 1-λ scattering data could introduce undesired noise. Moreover, at SIR and CMN, the σ_{sp} is measured with the single wavelength Ecotech nephelometer model M9003 (until 2013 at CMN). The correction curve from Müller et al. (2009; Figure 4) provides a correction factor of around 0.97 to 1.0 for the M9003 for a SAE of around 1.5 to 2. Using the TSI3563 scattering measurements performed at CMN during 2014-2015, we estimated a mean SAE of around 2 for CMN (cf. Table S5). Thus, given the rather small effect of the correction factor estimated for the Ecotech M9003, scattering data from CMN and SIR were not corrected in this work. At FKL the nephelometer models RR M903 (until 2011) and Ecotech 1000 (from 2012) were used (cf. Table 1). To the best of our knowledge, no correction scheme has been provided for the Ecotech 1000. Moreover, at FKL, the inlet was changed many times (cf. Table 1) and the correction factors provided in the literature are a strong function of the size cut-off used. For these reasons, scattering data collected at FKL are not corrected in this investigation.

2.2.2.2 Relative humidity

The integrating nephelometer measurements within ACTRIS and WMO-GAW should be performed at a low relative humidity (RH<40%) in order to avoid enhanced scattering due to water uptake of aerosol particles and in order to make the measurements comparable. For the Ecotech integrating nephelometers, the RH threshold can be set by using a processor-controlled automatic heater inside the instrument. At some mountain sites, where whole air is sampled (cf. Table 1), the natural temperature difference between the outside and inside air dries cloud droplets to the aerosol phase when a cloud is present at the station. RH is also controlled by de-humidifying in the inlet pipe, as reported in GAW report 226, to ensure a sampling RH of less than 40%. This recommendation is intended to ensure that the data are comparable across the network, as measurements would otherwise would be a strong function of the highly variable sample RH. Currently, at the majority of ACTRIS observatories, the aerosol particle light scattering measurements are performed at a RH

below 40%. However, given that at some stations the 40% RH threshold is sometimes exceeded, we selected in this work a RH threshold of 50% in order to improve the data coverage.

Estimating the aerosol particle light scattering enhancement due to an increase of RH from 40% to 50% is difficult using the data available here because the σ_{sp} measurements at a RH>40% are not evenly distributed over the measurement periods, with the majority of the stations registering a RH higher than 40% during the summer. Moreover, the chemical composition of atmospheric aerosol particles is an important factor determining the magnitude of the scattering enhancement due to water uptake, which can then change from one site to another (e.g. Fierz-Schmidhauser et al., 2010a,b; Zieger et al., 2014, 2017). However, the scattering enhancement due to a change in RH between 40% and 50% should be small and will not exceed few percent even for more hygroscopic particles (e.g. Fierz-Schmidhauser et al., 2010a,b). Table S2 in the Supporting Material reports the percentage of hourly σ_{sp} values collected in the range 40%<RH<50% whereas the frequency distributions of the measured RH are shown in Figure S1.

2.2.2.3 Available wavelengths

In this work we present and discuss the σ_{sp}, backscatter fraction (BF) and asymmetry parameter (*g*) measurements obtained using the green wavelength of the integrating nephelometers. The available wavelengths ranged from 520 nm (2 stations; CMN and VHL) to 550 nm (18 stations). Other wavelengths used are 525 nm (6 stations) and 532 nm (used at FKL until 2010; cf. Table 2). An exception is SIR, where only σ_{sp} values at 450 nm are available. The measurements of σ_{sp} reported here are not adjusted to 550 nm, which is generally the most common wavelength (e.g. Andrews et al., 2011) because of the different data availability of σ_{sp} and SAE at the measuring stations. As discussed in the following sections, the SAE is calculated for σ_{sp} data higher than 0.8 Mm^{-1}, thus leading to different data coverage for σ_{sp} and SAE and preventing the adjustment of all measured σ_{sp} to 550 nm. Moreover, the SAE is not available at FKL and SIR (or at CMN until 2014) thus preventing any wavelength adjustment at these stations. Using the mean SAE calculated at those stations, where σ_{sp} is measured at wavelengths in addition to 550 nm (cf. Tables S4 and S5 in Supporting material), we estimate differences in the σ_{sp} values of less than 6% after adjusting to 550 nm. At FKL and SIR, where the SAE is not available, and assuming a reasonable SAE range between 1.5 and 1.0, the difference due to the adjustment to 550 nm is 4.9-3.0% at FKL and 26-18% at SIR. The higher difference at SIR is due to the fact that measurements at this station are performed at 450 nm. Finally, at CMN, the effect of the adjustment of σ_{sp} to 550 nm (from 520 nm) using a mean SAE of 2 (calculated using the 3-λ nephelometer data from 2014; cf. Table S5) is below 10%.

1 **2.2.3 Calculation of aerosol particle intensive optical properties**

2 Starting from the spectral σ_{sp} measurements performed at the ACTRIS observatories, three
3 intensive aerosol particle optical parameters can be estimated, namely; the scattering Ångström
4 exponent (SAE), the backscattering fraction (BF) and the asymmetry parameter (*g*). These
5 intensive properties do not depend on the PM mass concentration and are directly related to
6 aerosol particle properties such as size, shape, size distribution and chemical composition. The
7 SAE can be considered as a proxy for the aerosol particle size range with a higher (lower) SAE
8 associated with predominance of fine (coarse) aerosol particles (e.g. Seinfeld and Pandis, 1998;
9 Esteve et al., 2012; Valenzuela et al., 2015 among others). The BF and *g* parameters are
10 calculated quantities that influence the variability of the radiative forcing efficiency and that
11 represent the angular light scattering of aerosol particles. For computational efficiency, the angular
12 light scattering is often represented by a single value (BF, σ_{sp}/σ_{bsp} or *g*) (Andrews et al., 2006).

13 The SAE characterizes the wavelength dependency of σ_{sp} and it can be calculated as follows:

$$ SAE = -\frac{\log\left(\sigma_{sp}^{\lambda_1}\middle/\sigma_{sp}^{\lambda_2}\right)}{\log\left(\lambda_1\middle/\lambda_2\right)} \quad . \qquad\qquad \text{(Eq. 1)} $$

15 Here, the SAE is derived from a multispectral log linear fit based on the three nephelometer
16 wavelengths. The SAE depends on the particle size distribution and takes values greater than 2
17 when the light scattering is dominated by fine particles (radii ≤ 0.5 μm as e.g. in Schuster et al.
18 (2006)), while it is lower than one when the light scattering is dominated by coarse particles
19 (Seinfeld and Pandis, 1998; Schuster et al., 2006).

20 The asymmetry parameter (*g*) (Andrews et al., 2006; Delene and Ogren, 2002) describes the
21 probability that the radiation is scattered in a given direction and it is defined as the cosine-
22 weighted average of the phase function. Thus, *g* yields information regarding the amount of
23 radiation that a particle scatters in the forward direction compared to the backward direction.
24 Theoretically, the values of *g* can range from −1 for only back scattering to +1 for complete forward
25 scattering, with a value of 0.7 commonly used in radiative transfer models. The *g* parameter can be
26 estimated from the backscatter fraction (BF), which is the ratio of σ_{bsp} and σ_{sp} (Andrews et al.,
27 2006):

28 $$ g = -7.14(BF)^3 + 7.46(BF)^2 - 3.96(BF) + 0.9893 \quad . \qquad\qquad \text{(Eq. 2)} $$

30 **2.2.4 Data coverage**

31 Table S3 in the Supporting Material reports the percentage [%] of data coverage at the 28 ACTRIS
32 stations included in this study. Removed data include data flagged as non-valid by the data

providers (instrument failure, calibration periods, unspecified contamination or local influence, etc.) or obtained at a RH of greater than 50%. The data coverage for the extensive measured aerosol particle optical properties (σ_{sp} and σ_{bsp}) is generally high, ranging from around 60% to 95%. Exceptions are the σ_{sp} measurements at CMN in the blue (450 nm) and red (700 nm) wavelengths which have much less data coverage compared to the green wavelength because the three wavelength nephelometer was implemented at CMN in 2014. Consequently, also the SAE and *g* have low data coverage at CMN. Moreover, lower data coverage (< 40%) was registered at PLA and VHL.

The data coverage for the intensive aerosol particle optical properties (SAE and *g*) is generally lower compared to the data coverage of σ_{sp} and σ_{bsp}. This is because the intensive optical properties are calculated from hourly σ_{sp} and σ_{bsp} data higher than 0.8 Mm^{-1} to avoid noise in the calculations. As a consequence, the data coverage of the intensive properties is lower at those stations measuring low σ_{sp} and σ_{bsp} values (e.g. mountain and remote sites). For example, at JFJ, the SAE and *g* data coverages are around 54% and 22%, respectively. At TRL, these values are even lower, at 21% and 1%, respectively. However, as reported in Table S3, at the majority of the stations the data coverage of SAE and *g* is higher than 60%.

3. Results/Discussion

3.1 Variability of σ_{sp}

Figure 2 shows the box-and-whiskers plots of σ_{sp} measured at the stations included in this investigation. In Figure 2, the observatories are grouped based on their placement and ordered according to their geographical location. Table S4 and Figure S2 in the Supplementary Material report, respectively, the statistics of σ_{sp} (mean, standard deviation, minimum and maximum values and 5th, 25th, 50th, 75th, and 95th percentiles) and frequency and cumulative frequency distributions.

In each geographical sector, an increasing gradient of σ_{sp} is generally observed when moving from mountain to regional and to urban sites. Thus, the σ_{sp} values measured at mountain sites are lower than the measurements made at other locations (coastal to urban) even if exceptions are observed in some sectors.

A large range of σ_{sp} coefficients is observed across the network, ranging from median values lower than 10 Mm^{-1} to values higher than 40 Mm^{-1}. Overall, the lowest σ_{sp} is on average measured at remote stations because of either: a) their altitude, for example JFJ is located in Central Europe at more than 3500 m a.s.l. and CHC in Bolivia is at around 5300 m a.s.l. (cf. Figure S3), or b) because of their large distance from pollution sources, for example the Arctic ZEP and PAL stations, TRL station (cf. Figure S3) and some regional sites in the Nordic and Baltic sector such

as BIR and SMR. Higher σ_{sp} values (medians > 40 Mm^{-1}) are on average registered at more polluted sites, such as some urban sites in Southern Europe (UGR and DEM), some regional sites in Eastern and Central Europe (KPS and IPR, respectively) and one coastal site in the Nordic and Baltic sector (PLA).

The observed variation is consistent with the differences in particulate matter (PM) mass concentrations, PM chemical composition, particle number concentration and absorption coefficients observed across Europe, as described for example by Putaud et al. (2010), Asmi et al. (2011) and Zanatta et al. (2016).

Figures 3a and 3b show the relationship between the mean particle number concentration measured at different stations during 2008 to 2009 (and reported in Asmi et al. (2011)) and the mean σ_{sp} measured over the same period (where available). As reported in Figure 3, good correlations are observed between N50 (Figure 3a: mean/median particle number between 50 nm and 500 nm) and N100 (Figure 3b: mean/median particle number between 100 nm and 500 nm) and mean σ_{sp}. Figure 3c shows the relationship (for some stations) between absorption coefficients reported in Zanatta et al. (2016) and the total scattering. The good correlations reported in Figure 3c (especially high for the winter and autumn periods) suggest an increase of both scattering and absorption coefficients with increasing aerosol loading.

Finally, at all stations included in this work, the skewness of the σ_{sp} distributions (cf. Table S4) is higher than one and ranges between 1.4 at PLA and 10.6 at TRL (skewness calculated from hourly averaged data). The skewness is defined as the third standardized moment of a probability distribution and it is a measure of the asymmetry of the probability distribution. Its value can be positive or negative. Positive skewness is usually observed for parameters which are defined to be positive and it indicates that the tail on the right side of the distribution is longer or fatter than that on the left side. Thus, for a right-skewed distribution, the mass of the distribution is concentrated on the left, and there is a higher probability of measuring a high value compared to a left-skewed distribution. Figure S2 in the Supporting Material shows the frequency and cumulative frequency distributions for σ_{sp} for each station, evidencing the presence of these right-skewed tails.

3.1.1 σ_{sp} at Arctic/Antarctic observatories

The Arctic (ZEP and PAL; cf. Fig 2) and Antarctic (TRL; cf. Figure S3) monitoring stations are located in undisturbed environments with minimal influence from the local settlement because they are located above the inversion layer. The mean σ_{sp} values measured at ZEP and TRL are by far the lowest across the network, whereas higher σ_{sp} values are measured at PAL. PAL is located in a remote continental area characterized by the absence of large local and regional pollution sources (e.g. Aaltonen et al., 2006). However, Lihavainen et al. (2015a) reported that high values of the absorption coefficient and low values of the single scattering albedo at PAL are related to

1 continental air masses from lower latitudes. Despite this, the mean σ_{sp} at PAL is among the lowest

2 in the ACTRIS network and is comparable to the mean σ_{sp} observed at the JFJ and CHC

3 mountaintop observatories (cf. Table S4).

3.1.2 σ_{sp} at mountain observatories

6 Differences can be observed among stations with similar environments but different geographical

7 locations. For mountain observatories, a clear gradient is not observed when moving from West to

8 Southeast Europe, because the altitude of the station is an important parameter contributing to the

9 σ_{sp} measured at these observatories. Among the mountain stations a higher mean σ_{sp} is on

10 average measured at HPB and IZO (cf. Table S4). The HPB station is likely to be more influenced

11 by the PBL than other mountain stations due to its lower altitude (Nyeki et al., 2012; Collaud Coen

12 et al., 2017), whereas IZO is largely influenced by Saharan dust outbreaks transporting dust

13 toward the station (e.g. Rodriguez et al., 2011) thus increasing σ_{sp}. In fact, at IZO, the median

14 value of σ_{sp} is among the lowest measured at these mountain sites (around 7 Mm^{-1}; cf. Table S4)

15 indicating that the sporadic but extremely intense pollution episodes due to Saharan mineral dust

16 outbreaks strongly affect the mean σ_{sp} at this station.

17 Despite their placement at higher altitudes, both CMN and BEO (more than 2 km a.s.l.) register

18 similar σ_{sp} values compared to PUY and MSA (around 1.5. km a.s.l.) likely because the effect of

19 important regional pollution sources (i.e. the Po Valley for CMN) affecting, under favourable

20 meteorological conditions, these Central and Eastern European observatories (i.e. Marenco et al.,

21 2004). Conversely, the region around the MSA observatory is sparsely populated and the station is

22 isolated from large urban and industrial agglomerations (i.e. Pandolfi et al., 2014; Ripoll et al.,

23 2014; Ealo et al., 2016). PUY observatory is surrounded by a protected area with fields and forests

24 and previous works have shown that the influence of the Clermont-Ferrand city on the PUY

25 measurements remains too small to be detected (i.e. Asmi et al. 2011).

26 The lowest median σ_{sp} values at mountain sites are on average measured at JFJ, probably due to

27 the higher altitude of this station compared to other mountain stations included in this work and/or

28 its distance from important pollution sources. Moreover, Collaud Coen et al. (2017) reported a low

29 PBL influence at this site due to the location of the station in a dominant position within the whole

30 mountainous massif. CHC (cf. Figure S3) registers higher median σ_{sp} values compared to JFJ

31 despite its location at around 5300 m a.s.l. likely due to the influence of the emissions from the city

32 of La Paz (3600 m a.s.l.), located around 30 km from the CHC site, and the local topography,

33 which facilitates the uplift of air masses toward the CHC observatory (Collaud Coen et al., 2017).

3.1.3 σ_{sp} at coastal observatories

The PLA coastal station registered σ_{sp} values which are higher compared to both other Nordic and Baltic stations and other coastal sites (e.g. MHD and FKL) and which are amongst the highest in Europe. Kecorius et al. (2016) have shown that ship emissions in the Baltic Sea contribute strongly to pollution levels at PLA and that up to 50% of particles arriving at PLA are generated by processes and emissions, including shipping, taking place in areas upwind of the station. Moreover, Asmi et al. (2011) presented a number of similarities in particle number concentrations measured at PLA to those measured at some Central European sites, such as IPR, which are due to the influence of multiple source areas (cf. Figure 3). It should be noted however, that the period with available σ_{sp} measurements is very short at PLA (cf. Table 1 and Figure 7) and the data coverage is also low (cf. Table S3). Consequently, more measurements at this site are needed in order to confirm the σ_{sp} values reported there. The other two coastal stations (MHD and FKL) register median σ_{sp} values in the upper range of σ_{sp} measured across the network, mostly due to the contribution of marine aerosols in winter and mineral dust in summer at MHD and FKL, respectively (cf. Paragraph 3.5).

3.1.4 σ_{sp} at regional/rural observatories

Regional sites exhibit a large variability in σ_{sp} coefficients across Europe, with the lowest values measured at BIR and SMR (Nordic and Baltic) and the highest at IPR (central Europe) and KPS (Eastern Europe). Thus, a gradient is observed in σ_{sp} when moving from West to East Europe. At both IPR and KPS, the frequent winter time episodes, linked to stable air due to strong thermal inversions, affect the level of pollution at these sites (e.g. Putaud et al., 2014; Molnár et al., 2016). It is known that at the IPR station, even though it lies several tens of kilometres away from large pollution sources, is located in an area (the Po Valley) which is one of the most polluted regions in Europe (e.g. van Donkelaar et al., 2010). The VHL observatory registers an on average higher σ_{sp} compared to PAL and compared to the BIR and SMR regional sites likely because VHL is located closer to the European continent and it is consequently more affected by polluted continental air masses. Moreover, the emissions from the densely populated areas of Helsingborg and Malmö and the city of Copenhagen, located 25 km to the west, 50 km to the south and 45 km to the south-east, respectively, could also explain the relatively high σ_{sp} measured at VHL (Kecorius et al., 2016). The σ_{sp} values at a regional level in Western Europe (OPE and CBW) are on average higher compared to those measured in the Nordic and Baltic regions and lower compared to those measured at a regional level in Southern Europe (MSY). The relatively higher σ_{sp} values measured at MSY are due to both the contaminated air transported by the sea breeze from the close metropolitan area of Barcelona to the mountains and the frequent Saharan dust outbreaks (i.e. Pandolfi et al., 2011; 2014a).

3.1.5 σ_{sp} at urban/sub-urban observatories

Among the urban background sites, lower σ_{sp} values are measured at MAD and SIR compared to DEM and UGR. The low σ_{sp} at MAD during the period presented here (only 2014 data are available for MAD) could be related to the reduced formation of secondary nitrate aerosols due to the limited availability of ammonia in this urban environment (Revuelta et al., 2014). However, it should be noted that winter episodes with high secondary nitrate concentrations are not uncommon in Madrid and we are presenting here only one year of measurements for this station. On the other hand, secondary inorganic aerosol concentrations recorded at the SIR sub-urban observatory can be considered as representative of a large geographical zone, given the rather flat orography of the Parisian basin. At UGR, the accumulation, mainly in winter, of fine particles from traffic, domestic heating and the burning of biomass explains the relatively higher σ_{sp} (e.g. Lyamani et al., 2012; Titos et al., 2017). Traffic emissions, the high level of formation of secondary sulphate and organic aerosols in the summer and the transport of dust from Africa are the main contributory factors to the high σ_{sp} at DEM where high $PM_{2.5}$ and PM_{10} values are usually measured as compared to other important Mediterranean cities (e.g.: Diapouli et al., 2017; Eleftheriadis et al., 2014; Karanasiou et al. 2014; Querol et al., 2009).

3.2 Variability of SAE

Figure 4 shows the box-and-whiskers plots of the SAE calculated at the different stations. Table S5 and Figure S4 in the Supplementary Material report the statistics of the SAE and frequency and cumulative frequency distributions, respectively. It should be noted that any comparison of the SAE values among the different stations could be slightly biased by the different particle size cuts upstream of the integrating nephelometers used in this work (cf. Table 1). Currently, all ACTRIS integrating nephelometers measure whole air or PM_{10}, with the exception of SIR, where the PM_1 inlet is used. Whole air is currently measured at mountain observatories (BEO, CMN, JFJ, PUY, CHC), one coastal observatory (MHD) and one urban observatory (UGR) (cf. Table 1).

At some stations, the inlet was changed from whole air to PM_{10} at some point, namely at OPE, FKL and TRL. Given the lower scattering efficiency of aerosol particles larger than 10 μm, no important differences in the SAE should be expected between aerosol particles sampled with a whole air and a PM_{10} cut-off. At the other stations the inlet was changed during the measurement period from a cut-off lower than 10 μm (1 μm at KPS; 2.5 μm or 5 μm at PAL, MSA and MAD) to PM_{10}. For PAL (where a median SAE of around 1.8 was measured; cf. Table S5), Lihavainen et al. (2015a) assumed that the inlet changes (from PM_5 to $PM_{2.5}$ in 2005 and from $PM_{2.5}$ to PM_{10}, cf. Table 1) had only minor effects on scattering because the number concentration of coarse particles is very low at PAL. Similarly, the KPS observatory registers among the highest SAE values observed in the network (median value of around 2) suggesting an aerosol particle size distribution dominated by fine particles. Consequently, the inlet change from PM_1 to PM_{10} at KPS had probably

only a minor effect on SAE. Finally, two stations (MSA and MAD) changed the inlet from a $PM_{2.5}$ diameter cut-off to PM_{10}. For these two Southern European stations the inlet change may have had an effect on the SAE, especially during Saharan dust outbreaks, which are however sporadic events. Thus, despite the differences in the particle diameter cut-off, the comparison between the different stations in terms of SAE seems feasible.

3.2.1 Variability of SAE by geographical sector

The SAE shows a large variability across the geographical sectors considered in this study (Figure 4). On average, independently from of the station setting, the highest SAE is observed at the Central and Eastern European observatories (cf. Table S5) with station-averaged values of 1.88 ± 0.49 and 1.88 ± 0.53, respectively. The high SAE values in Central and Eastern Europe indicate clearly the predominance of fine particles. In fact, high $PM_{2.5}/PM_{10}$ ratios, indicative of the presence of small particles, are typical for rural lowland sites in Central Europe (e.g. Spindler et al., 2010; EMEP, 2008). Figure S4 shows that the frequency plots of SAE data have very similar unimodal delta-like distributions and the variability of the SAE within the 5th to the 95th percentile range is much lower than that of the other European regions, suggesting a greater homogeneity in some microphysical properties of atmospheric particles such as size. Exceptions are the CMN, JFJ and BEO mountain sites, where left-tailed SAE distributions are observed, likely due to the reduced effect of fine particles from the PBL in winter and an increase in the relative importance of coarse mineral dust, sea salt particles as well as aged aerosols compared to lower altitude stations in the same geographical sector.

On average, the SAE is lower for all other geographical sectors. Station-averaged mean SAE of around 1.60 ± 0.61, 1.25 ± 0.86 and 1.36 ± 0.67 are observed in the Nordic and Baltic, Western and Southwestern sectors, respectively. Exceptions are however observed. For example, at CBW (Western Europe) the median SAE reaches values of around 2.1. Indeed, both polluted air masses from the industrialized zones of the Benelux countries and clean air masses from the sea contribute to the presence of aerosol particles at this site (Crumeyrolle, et al., 2010). Moreover, CBW is surrounded by several large cities at distances of approximately 20 to 40 km from the station, which may have contributed to the high SAE values measured in this geographical location. Asmi et al. (2011) have also shown that background particle number concentrations at CBW are much higher than, for example, at BIR.

Median SAE values close to one or lower, indicative of the fact that the σ_{sp} is dominated by large particles, are observed at remote sites in Western Europe (MHD), Southwestern Europe (IZO) and the Nordic and Baltic (ZEP) and Antarctic (TRL) regions. A low SAE at MHD has already been reported by Vaishya et al. (2011, 2012) and justified by the frequent presence, mainly in winter, of coarse-mode sea-salt particles, since mineral dust particles can be ruled out. In fact, air masses originating from dust sources are infrequent at these sites. Similarly, the low SAE observed at ZEP and TRL can be associated with the presence of coarse sea-salt particles (e.g. Zieger et al., 2010 for ZEP). Conversely, the SAE obtained at IZO is mainly due to the frequent

presence of mineral dust particles from African deserts (e.g. Rodríguez et al., 2011). Very similar bi-modal frequency distributions are observed at MHD and IZO, showing a pronounced left peak indicative of the high probability of encountering coarse particles at these sites. BIR and PLA also show an enhanced left peak in the SAE frequency distributions likely due to the presence of coarse marine aerosols at these sites.

3.2.2 Variability of SAE by station type

Unlike σ_{sp}, the SAE does not show any clear gradient when moving from mountainous to regional/urban sites in each geographical sector. For example, at mountain sites the median SAE ranges between around 0.7 at IZO (Southwest Europe) and values higher than two at JFJ and CMN (Central Europe). As reported by Zieger et al. (2012) a SAE value of around 2 prevails for most of the time at JFJ and can be regarded as the typical background under non-dusty conditions. Thus, the SAE values at JFJ and CMN can be considered as representative of Central Europe's free troposphere, especially in winter when the PBL emissions at these sites are reduced. This high variability of SAE at mountain sites was also reported by Andrews et al. (2011) with values from 11 mountaintop stations worldwide ranging from less than one to more than two. Moreover, Bourcier et al. (2012) have shown that coarse particles are transported more efficiently at high altitude by the higher wind speed, thus probably also contributing to the observed variability of SAE at mountain sites.

Also at coastal sites (PLA and MHD), the SAE shows large variability, with higher SAE measured at PLA compared to MHD, confirming a higher effect of anthropogenic emissions at PLA compared to MHD.

An increasing gradient of SAE is observed when moving from regional/rural observatories in the Northwest of Europe to regional/rural observatories in the east of Europe. Among these stations, the lowest SAE is observed at VHL (Nordic and Baltic) and MSY (Southwestern Europe), whereas, as already observed, central and eastern regional areas are characterized by high SAE values. This gradient is also driven by the importance of sea salt or dust particle contributions affecting more the Northwestern and Southwestern European countries compared to countries in Central and Eastern Europe.

Among the urban sites, MAD registers the lowest median SAE (1.47) compared to UGR (1.69) and DEM (1.60). The lower SAE at MAD could be explained, as already noted, by the reduced formation of secondary inorganic aerosols during the available measurement period. Moreover, re-suspended dust from vehicles could also explain the lower SAE observed at the MAD observatory.

3.3 Variability of *g*

The asymmetry parameter is widely used in radiative transfer models because it provides information regarding how much radiation is scattered back compared to the amount of radiation scattered in the forward direction. Figure 5 shows the box-and-whiskers plots of *g* calculated at the

different stations. Table S6 and Figure S5 in the Supporting Material report the statistics of *g* and the frequency and cumulative frequency distributions, respectively. Given that *g* is calculated from BF using Equation 2 (Section 2.2.3), we report in Figure S6 of the Supporting material the box-and-whiskers plots of BF, whereas Table S7 reports the statistics of BF. Figure 5 and Figure S6 are symmetrical, with a lower BF corresponding to a higher *g*.

3.3.1 Variability of *g* by geographical sector

Unlike the SAE, the *g* parameter does not show any clear gradient when moving from the west to the east of Europe. Slightly higher *g* values are observed in Western Europe (station-averaged mean *g* of 0.61 ± 0.08) compared to Central and Eastern Europe (mean *g* = 0.59 ± 0.07 and 0.57 ± 0.06, respectively). These differences in the g values, even if small, are consistent with the opposite gradient observed for SAE, this latter being smaller in Western Europe. However, the station-averaged *g* in Central and Eastern Europe is similar to the mean *g* observed in the Nordic and Baltic regions (mean *g* = 0.58 ± 0.08) and in Southwestern Europe (mean g = 0.57 ± 0.06). Thus, contrary to the SAE, a clear relationship between aerosol size and *g* is not observed. The possible reasons for this are reported below.

3.3.2 Variability of *g* by station type

At some mountain sites higher median *g* values are observed relative to the *g* values obtained at regional or urban locations. This is the case for example for IZO compared to MSY, UGR and MAD in the Southwestern European sector and for HPB and JFJ compared to IPR, MPZ and KOS in Central Europe. However, exceptions are observed. For example at CMN, where the median *g* value (only 2 years of data are available) is the lowest in the Central European sector and among the lowest observed in this study. On average, *g* values range between 0.49 and 0.64 at mountain sites, with a mean value of 0.58 ± 0.05. This value is consistent with the mean value of 0.61 ± 0.05 reported by Andrews et al. (2011) at the mountain sites included in their work.

Figure S7 in the Supporting Material reports the mean SAE (ordered from low to high values for each station setting) and *g* at each station used in this work together with the SAE-*g* scatter plot. Figure S7 shows that no clear relationship between *g* and SAE is observed. For example, the TRL and MHD observatories register among the highest *g* values observed in the network which is consistent with the very low SAE measured at these stations because of the frequent presence of coarse-mode sea-salt particles (cf. Figure 4). However, high *g* values, similar to TRL and MHD, are also observed at stations such as PLA, BIR, JFJ and DEM, which are dominated on average by fine aerosol particles (with SAE values similar to or higher than 1.5). Similarly, similar *g* values are observed at IZA and PUY or HPB despite the differences in SAE values at these observatories.

Differences in the shape of the particle number size distribution, particle shape and chemical composition (e.g. refractive index, RI) are likely factors contributing to the poor relationship observed between *g* and SAE. The Mie theory of polydisperse spherical particles predicts that the BF is lower and *g* correspondingly higher for coarse-mode aerosol particles (for which the SAE will

be low) compared to fine-mode particles. However, some studies deploying integrating nephelometers have found that the BF can be higher for coarse-mode aerosol particles (such as mineral dust) than for fine-mode aerosol particles (Carrico et al., 2003; Doherty et al., 2005). Doherty et al. (2005) suggested that an under-correction for the σ_{sp} truncation of the forward-scattered radiation (which is relatively larger for coarse particles) could bias the calculated BF toward high values. Moreover, the shape of the particle number size distribution is another factor affecting the BF and SAE. Thus, differences in the relative fractions of the fine and coarse modes could also drive the BF-SAE relationship. In fact, the SAE is most sensitive to the presence of coarse-mode aerosol particles compared to the BF, which is most sensitive to small accumulation-mode particles (Delene and Ogren, 2002; Collaud Coen et al., 2007). Thus, depending on the shape of the particle number size distribution, the BF and SAE values might or might not correlate.

The refractive index (RI), which is strongly related to the chemical composition of the particles, is another important variable that can affect g (e.g. Marshall et al., 1995). In the work of Hansen and Travis (1974; Figure 12) the authors showed that, for a given particle diameter, the g parameter non-linearly decreased with increasing real RI. Thus, coarse-mode particles with a given RI could have an asymmetry parameter similar to or lower than that of fine particles with lower RI. Recently, Obiso et al. (2017) confirmed the findings of Hansen and Travis (1974), showing also that for fine particles a perturbation in the RI of 20% has a larger effect on g than a similar relative perturbation of particle shape. Obiso et al. (2017) also showed that a variation of the RI for coarse particles can have a small effect on the mass scattering efficiency of a particle and its spectral dependence, and consequently also on SAE.

3.4 Seasonal variability

Figures 6, 7 and 8 present the annual cycles of σ_{sp}, SAE and g, respectively, at each site. The annual cycles for the non-European CHC and TRL stations are reported in Figure S8 in the Supporting Material. Overall, strong seasonal cycles of σ_{sp} and intensive aerosol particle optical parameters are observed at the majority of the stations, although exceptions are observed. The analysis of the annual cycles is presented below separately for different station settings.

3.4.1 Seasonal variability at Arctic observatories

ZEP and PAL observatories present quite different annual cycles of σ_{sp}. At ZEP, the highest σ_{sp} is observed in late winter and in spring whereas the lowest σ_{sp} is observed in the summer. The σ_{sp} values increase in late winter and spring due to the Arctic Haze phenomenon, i.e. layers with enhanced concentrations of aerosols and precursor gases in the Arctic troposphere caused by anthropogenic sources and long-range transport (i.e. Engvall et al., 2008; Ström et al., 2003). Ström et al. (2003) have shown that, during winter and spring, the aerosol particle accumulation-mode dominates. Conversely, in summer, this mode is significantly smaller and Aitken-mode-sized

aerosols dominate the size distribution. The change in the aerosol size distribution between winter/spring and summer is likely the cause of the observed variations of σ_{sp} and g at ZEP, the latter being slightly larger in late winter and spring compared to the summer. At PAL observatory, an on average higher σ_{sp} is observed in spring/summer compared to autumn/winter. As reported by Lihavainen et al. (2015a), low values of σ_{sp} in autumn and early winter can be related to frequent precipitation events, whereas the high values of σ_{sp} in summer are probably related to biogenic organic aerosols from natural sources. At PAL, the monthly variation of SAE and g is rather pronounced: SAE (g) increases (decreases) in summer compared to winter, indicating the predominance of relatively smaller particles during the warmest months. Lihavainen et al. (2015a) observed that the seasonal variations in intensive aerosol optical properties at PAL are related to both the transport of different air masses at this remote site depending on the season, and the enhanced formation of BSOA (biogenic secondary organic aerosols) in the summer. Lihavainen et al. (2015a) also reported a lower single scattering albedo in winter compared to summer at PAL due to a significant contribution from light absorbing carbon, mostly from residential wood combustion. Thus, they have shown that aerosol particles observed in the summer at PAL have the potential to cool the atmosphere more efficiently than those observed during winter.

3.4.2 Seasonal variability at mountain observatories

At the mountain stations (PUY, HPB, JFJ, CMN, BEO, MSA and IZO), the σ_{sp} peaks in spring/summer whereas lower σ_{sp} values are measured in autumn/winter. Similar findings were, for example, already reported by Nyeki et al. (1998) for JFJ and summarized by Andrews et al. (2011) for many mountain top stations worldwide and by Pandolfi et al. (2014) for MSA station. Different factors contribute to the σ_{sp} increase in spring/summer at the mountaintop observatories, such as the increase of the boundary layer height and the stronger upslope winds during the warmest months. Moreover, specific events, such as Saharan mineral dust outbreaks, may contribute to the increased σ_{sp} observed at mountain stations in spring/summer, especially in Southern Europe (e.g. Pey et al., 2013; Pandolfi et al., 2014; Rodríguez et al., 2011). At IZO, σ_{sp} peaks strongly in July-August because of the very high influence of African mineral dust at this station during these months (e.g. Alastuey et al., 2005; Diaz et al., 2006; Rodríguez et al., 2015). At the mountaintop CHC observatory (cf. Figure S8), σ_{sp} progressively increases during the dry season, from May to October, reaching lower values during the rainy season (from December to April). Moreover, during the dry season, the new particle formation events, taking place at CHC with one of the highest frequencies reported in the literature so far (Rose et al. 2015), can introduce very small particles that grow to nucleation and the Aitken mode.

At the mountain stations, both SAE and σ_{sp} are on average higher in summer compared to the winter period, thus suggesting a higher anthropogenic influence at these sites during the warmest months. The summer SAE increase is more evident at some mountain stations, e.g. HPB,

CMN and BEO, compared to other mountain stations such as JFJ and MSA. The less pronounced SAE seasonal variation at JFJ was related by Bukowiecki et al. (2016) to the rather constant composition of the JFJ aerosol. At MSA in Southwestern Europe, the observed less pronounced seasonal cycle of SAE could be due to the contribution of Saharan dust in spring/summer, which contrasts with the PBL transport of fine particles observed at other mountain sites during the warm season. At IZO, the SAE reaches its lowest values during July-August in conjunction with the peak frequency of dust events (Rodríguez et al., 2015).

Overall, the *g* parameter shows an opposite seasonal cycle compared to the SAE at almost all mountain stations, with the exception of JFJ and BEO, where *g* slightly increases with SAE in the summer. At almost all mountain stations, the seasonal variations of SAE and *g* are less pronounced compared to the seasonal variation of σ_{sp}, indicating a larger seasonal variation in the extensive aerosol optical properties than in the intensive properties. At CHC, the SAE decreases as the σ_{sp} increases when moving from the wet to the dry season, indicating an increasing effect of coarse particles on the σ_{sp} during the dry season. At PUY, σ_{sp} peaks from March to September and this increase is accompanied by a small increase in SAE. Venzac et al. (2009) and Boulon et al. (2011) have shown that PUY is more often influenced by the free troposphere or residual layers in winter and spring compared to the summer season.

3.4.3 Seasonal variability at coastal observatories

A very different seasonal variation of σ_{sp} is observed at the two coastal observatories, MHD and FKL (at PLA, the lack of spring/summer measurements prevents the analysis of the annual cycles). The σ_{sp} at MHD (Western Europe) peaks in winter, whereas a higher σ_{sp} is observed in summer at FKL (Southeastern Europe). At FKL, where no intensive optical aerosol properties are available, the higher σ_{sp} in summer can be associated with mineral dust storm events, such as reported by Vrekoussis et al. (2005). However, mineral dust storms in the Mediterranean are not the only reason for the observed increased σ_{sp} in the summer at FKL. In fact, as for example reported by Kalivitis et al. (2011), ammonium sulphate and particulate organic matter, whose concentrations increase in summer in the Mediterranean Basin, can also be assumed to be important contributors to σ_{sp} during the warm season. At MHD, the higher σ_{sp} in winter is related to the higher contribution of wind-speed-generated sea-salt particles in the marine boundary layer during winter time (Vaishya et al., 2011). At MHD, the SAE (*g*) is higher (lower) in summer compared to winter. O'Connor et al. (2008) and Vaishya et al. (2011, 2012) showed that the background marine aerosol level measured at MHD contains a strong and significant seasonal cycle with sea salt dominating in winter and biogenic organic aerosols dominating at the submicron scale in summer. This is consistent with the observed seasonal cycles of SAE and *g* reported here for MHD.

3.4.4 Seasonal variability at regional/rural observatories

Regional observatories in Central and Eastern Europe show marked seasonal cycles of both extensive and intensive aerosol particle optical properties. In these regions, less horizontal and vertical pollutant dispersion in winter, due to a higher frequency of stagnant conditions and temperature inversions, play an important role in the accumulation of aerosols. As a consequence, the σ_{sp} is much higher in winter compared to summer. SAE and g also show marked seasonal cycles in these regions, with the SAE (g) being higher (lower) in summer compared to winter. Ma et al. (2014) have shown that, at MPZ, an increased SAE in summer is mainly explained by the variation of the particle number size distribution. Thus, high concentrations in spring and summer of small particles during new particle formation and subsequent growth periods cause the observed increase of SAE (and correspondingly a decrease of g) during the warmest months.

At regional sites in the Nordic and Baltic region, the monthly variation of σ_{sp} is on average less pronounced compared to the Central or Eastern European stations, especially at BIR and SMR. This is likely due to the placement of these stations in remote areas with a different meteorology (e.g. less pronounced PBL variations) where on average much lower σ_{sp} values are measured compared to other European sites. Moreover, this could also indicate the importance of anthropogenic sources such as domestic heating in Central and Eastern Europe in winter. However, both SAE and g show marked seasonal cycles at these Nordic and Baltic observatories, similar to those reported for Central and Eastern European observatories with higher (lower) SAE (g) in summer compared to winter.

Differences are observed in the annual cycle of σ_{sp} at a regional level in Southwestern Europe (represented by the MSY observatory) where higher σ_{sp} values are registered in summer. At the MSY regional site (located at around 720 m a.s.l.), the higher efficiency of the sea breeze in transporting pollutants from the urbanized/industrialized coastline toward regional elevated inland areas during the warmer season mainly explains the summer increase in aerosol particle mass concentration and scattering coefficient observed at this site (e.g. Pandolfi et al., 2011). Moreover, the enhanced formation of secondary sulphate and organic matter in the summer, together with frequent Saharan mineral dust outbreaks, strongly contribute to the observed seasonal cycle for σ_{sp} and the intensive properties at the MSY site. The σ_{sp} peak observed at MSY in March is due to the winter pollution episodes typical of the western Mediterranean Basin (WMB) (e.g. Pandolfi et al., 2014a and references therein). During these episodes, the accumulation of pollutants close to the emission sources is favoured by anticyclonic conditions coupled with strong atmospheric inversions. During such conditions, pollutants accumulate in the PBL and can subsequently reach the MSY station when the PBL height increases.

3.4.5 Seasonal variability at urban/sub-urban observatories

Among the urban sites, marked variations of σ_{sp} and the intensive properties are observed at UGR and DEM. At the urban UGR site, the mean aerosol type is very different in winter compared to

summer. As evidenced by the seasonal cycles of SAE and g, aerosol particles are generally finer during the winter at UGR compared to the summer season, as already observed for example by Lyamani et al. (2010; 2012) and Titos et al. (2012). This is likely due to the accumulation of fine particles, mainly from traffic, domestic heating and biomass burning, favoured by stagnant conditions and atmospheric inversions during winter. In summer, the higher frequency of Saharan mineral dust outbreaks at this site increases the mean size of the particles during the warmest months. At the DEM urban observatories, the high σ_{sp} values measured in spring are linked to Saharan dust outbreaks, as also supported by the seasonal cycles of SAE and g which show the lowest and highest, respectively, values in spring.

3.5 SAE and g vs. σ_{sp} relationships

Figure 9 shows the relationships between σ_{sp} and SAE and between σ_{sp} and g at each station. Mean SAE and g are calculated for each σ_{sp} bin and the bin size at each station is calculated following the Freedman–Diaconis rule:

$$\text{Bin size} = 2\frac{\text{IQR(x)}}{\sqrt[3]{n}} \qquad , \qquad\qquad\qquad\qquad\qquad \text{(Eq. 3)}$$

where IQR(x) is the interquartile range of the data and n is the number of observations in the sample x. These graphs help in understanding which aerosol type on average dominates the particle light scattering, depending on the degree of scattering measured. It should be noted that, in Figure 6, the number of samples available at each station is not evenly distributed among the considered bins. Figure S9 in the Supplementary Material shows, for some stations, the SAE-σ_{sp} pairs coloured by the number of samples in each bin to highlight how the samples are distributed amongst the bins.

3.5.1 g-σ_{sp} relationships

The asymmetry parameter g shows the lowest values for very low σ_{sp}, suggesting the predominance of small fine-mode particles. Andrews et al. (2011) reported similar g-σ_{sp} relationships at different mountain sites and suggested that the removal of large particles by cloud scavenging or by deposition during transport could explain the observed low g values in a clean atmosphere. They also suggested that the formation of new particles followed by condensation/coagulation could generate small but optically active particles. Here, we show that this behaviour of BF or g as a function of σ_{sp} was observed at all sites, not only at mountain sites.

The parameter g then increases with increasing σ_{sp}, indicating a shift of the particle number size distribution toward the larger end of the accumulation mode. Delene and Ogren (2002), Andrews et al. (2011), Pandolfi et al. (2014) and Sherman et al. (2015) showed that the BF tends to decrease with increasing aerosol loading, consistent with the observed increase of g. For comparison with

previous works, Figure S10 in the Supplementary Material shows the BF-σ_{sp} relationships for all observatories, evidencing the aforementioned BF decrease with increasing σ_{sp}.

The shift of the particle number size distribution toward the large end of the fine mode with increasing σ_{sp} is probably the main reason causing the observed increase of g (and the decrease of BF, cf. Figure S10). A possible explanation for this shift is a progressive aging of atmospheric aerosol particles. Then, at the majority of stations, the variation of g is less pronounced during periods of high particle mass concentration, suggesting changes mostly in the coarse aerosol particle mode rather than in the fine mode.

3.5.2 SAE-σ_{sp} relationships

As reported in Figure 9, at some stations the SAE progressively increases with σ_{sp} in the σ_{sp} range where the g parameter also increases. The increase of both g and SAE with σ_{sp}, observed for example at the Nordic and Baltic regions, and Central and Eastern European observatories, could be related to the different effects that different particle sizes have on the SAE and g. A progressive increase of SAE with σ_{sp} would suggest an increasing relative importance of fine aerosol particles. The origin of these fine particles is probably different depending on the location of the measuring site. For the remote PAL site, for example, Lihavainen et al. (2015b) observed an increase of both σ_{sp} and SAE with increasing temperature due to the increasing rate of formation of BSOA with increasing ambient temperature, thus likely driving the σ_{sp}-SAE relationships reported in Figure 9 for PAL. The BSOA from gas-to-particle formation over regions substantially lacking in anthropogenic aerosol sources, such as the European boreal region (Tunved et al., 2006), probably contribute strongly to the σ_{sp}-SAE relationships observed at other Nordic and Baltic sites, such as SMR. At polluted sites, such as those located in Central and Eastern Europe, the anthropogenic aerosol emissions and active secondary aerosol production in the region (e.g. Ma et al., 2014) are probably driving the σ_{sp}-SAE relationships reported in Figure 9.

For higher σ_{sp}, the σ_{sp}-SAE relationships change and a progressive shift toward relatively larger particles is on average observed with increasing σ_{sp}. However, at the majority of Northwestern, Central and Eastern European stations, the SAE maintains values around, or higher than, 1.5 at high particle loads, indicating that the high σ_{sp} is dominated by fine particles. An exception is MHD, where the SAE increases with increasing σ_{sp}, maintaining values on average lower than 1.4 at high particle loads (cf. Figure 9). As already observed, the low SAE at MHD is mainly due to the predominance of sea-salt coarse particles at this site (Vaishya et al., 2011). Conversely, at some sites in Southern Europe (e.g. MSA, MSY, IZO, DEM) the SAE reaches values of around one or lower for high particle loads, indicating that, at these stations, the high σ_{sp} is dominated by mineral dust coarse particles mainly from African deserts. Exceptions are two urban sites in Southwestern Europe (UGR and MAD) where fine particles, probably generated for

the most part by traffic (and also from biomass burning at UGR) on average dominate the highest measured σ_{sp} values.

Similar σ_{sp}-SAE relationships to those reported in Figure 9 were observed by Andrews et al. (2011) at mountain sites and by Delene and Ogren (2002) at marine sites. Among the lowest SAE are observed at IZO, the station closest to the African continent. Interestingly, at IZO, the SAE shows the highest gradient for σ_{sp} coefficients in the range of 0 to 50 Mm^{-1} whereas the gradient is much lower for σ_{sp} values higher than 50 Mm^{-1}, with the SAE being almost constant for σ_{sp} higher than 100 Mm^{-1}. The IZO station is often in the free troposphere and high loadings at this station are only registered during Saharan dust events, thus it is virtually only the mineral dust that is measured at IZO. Normally, the long-range transport mineral dust particles do not represent a significant fraction of the particle population above 10 µm because of their short lifetimes, which likely explains the constant SAE observed at the IZO site under high aerosol loading.

3.6 Trends

Trends of σ_{sp}, SAE and BF are studied for those stations having more than 8 years' worth of data (13 observatories). Among the ACTRIS stations, PAL, SMR, MHD, HPB, IPR, JFJ and UGR have more than 10 years of data, whereas at PUY, MPZ, CMN, BEO, KPS and IZO, 8 or 9 years of data are available. These stations are included in order to improve the spatial coverage, as is the case in Collaud Coen et al. (2013). The Theil Sen statistical estimator (Theil, 1950; Sen, 1968) is used here to determine the regression parameters of the data trends, including slope, uncertainty in the slope and p-value. The Theil Sen method provides similar results to the Mann-Kendall test and it is implemented for example in the Openair Package available for R software (Carslaw, 2012; Carslaw and Ropkins, 2012). The applied method yields accurate confidence intervals, even with non-normal data, and it is less sensitive to outliers and missing values (Hollander and Wolfe, 1999). Monthly means are used for trend analysis and the data are corrected for seasonal effects.

The data coverage for σ_{sp} is higher than 70% at all stations included in the trend analyses with the exception of IZO, where the σ_{sp} data coverage is 55%. For SAE, the data coverage is higher than 65% at all sites with the exception of PAL (54%), PUY (59%) and IZO (52%). For BF, the data coverage is higher than 65% with the exception of PAL (26%), PUY (43%), BEO (47%) and IZO (27%). At the remote (PAL) or mountain stations (PUY, BEO and IZO), the percentage for the intensive aerosol particle optical properties is lower because there is a higher probability of measuring σ_{sp} lower than the threshold (0.8 Mm^{-1}) selected for the calculation of SAE and BF.

Table 2 reports the trends observed for σ_{sp}, SAE and BF at the thirteen observatories included in this analysis. Magnitude and statistical significance of the trends for these parameters are reported in Table S8 in the Supporting Material. It should be noted that changes in the particle

size cut-off reported for PAL and KPS (cf. Table 1) may have affected the reported trend analyses at these stations, but estimating the impact of these changes in the observed trend is not simple. However, as already noted, Lihavainen et al. (2015a) reported that, at PAL, the inlet changes had minor effects on scattering because the number concentration of coarse particles is very low at this observatory. KPS is dominated by very fine particles and the change from PM_1 to PM_{10} had probably only a minor effect on σ_{sp}, SAE and BF. Moreover, at KPS, the inlet was changed in April 2008, less than 1.5 years after the measurements commenced, and thus likely has also a minor effect in the trend analysis performed at this site over the period 2006 to 2014. The FKL observatory was removed from the trend analysis because the inlet was changed from whole air to PM_{10} in 2009, from PM_{10} to PM_1 in 2011 and again from PM_1 to PM_{10} in 2013 (cf. Table 1). These events likely had a major effect on the measured particle optical properties.

In Table 2, comparisons with the previous trend analysis results presented by Collaud Coen et al. (2013) for aerosol particle optical properties and by Asmi et al. (2013) for particle number concentrations are also reported.

3.6.1 Trends of σ_{sp}

Overall, a statistically significant decreasing trend for σ_{sp} is observed at around 50% of the stations considered here (Table 2). Significantly, decreasing trends for σ_{sp} are observed at the two Nordic and Baltic observatories (PAL for the period 2000 to 2010 and SMR); at two observatories (HPB and IPR) out of the five observatories in Central Europe; and at the two observatories in Southwestern Europe (IZO and UGR). The trends are not statistically significant in Western (MHD and PUY) and Eastern (BEO and KPS) Europe. The highest magnitude for the σ_{sp} trend [Mm^{-1}/yr] (cf. Table S8 in the Supplementary Material) is observed at the polluted IPR observatory. Conversely, the lowest magnitude is observed at the remote PAL observatory.

For the periods considered in this work, the total reductions (TR) for σ_{sp} range between approximately 30% (SMR) and 60% (IZO). The high TR observed at IZO might be affected by the intensity and frequency of Saharan dust outbreaks at this site. However, estimating the effects of these events at IZO is beyond the scope of this study. Overall, the observed decreasing trends of σ_{sp} are consistent with a uniform decrease in the aerosol optical depth observed in Europe (AERONET data in Li et al., 2014).

The observed statistically significant and decreasing trends of σ_{sp} are consistent with the demonstrated reduction of PM concentration in the atmosphere in Europe in recent decades thanks to the implementation of European/national/regional/local mitigation strategies. These decreasing trends are also consistent with the trends in the aerosol chemistry derived from observations in urban environments in Europe (e.g. EEA, 2013; Barmpadimos et al., 2011; Titos et al., 2014; Pandolfi et al., 2016), regional and remote environments in the western Mediterranean

(Cusack et al., 2012; Pandolfi et al., 2016) and in general with trends derived for the aerosol chemistry across Europe (Tørseth et al., 2012). Recently, Collaud Coen et al. (2013) showed that trends in σ_{sp} are observed at most of the US continental sites and that these trends are generally consistent with the strong SO_2 and PM reductions observed in the United States (Asmi et al., 2013; EPA, 2011). Conversely, in Europe, the strong decreasing trend observed for SO_2 (e.g. Tørseth et al., 2012; Henschel et al., 2013) and, with a lower spatial homogeneity and statistical significance, for $PM_{2.5}$ (e.g. EEA, 2016) is not observed for aerosol optical properties. As reported in Collaud Coen et al. (2013) the reasons that at some of the European sites no significant trends are observed, might be related to the spatial inhomogeneities and under-representation of continental Europe PBL sites (e.g. Laj et al., 2009) and/or the timing of the SO_2 and PM trends for the United States and Europe. In Europe, the emission reductions were greater for the period 1980 to 2000 compared to the period 2000 to 2010 (e.g. Colette et al., 2016; Tørseth et al., 2012; Manktelow et al., 2007), thus the measurements of optical particle properties in Europe may not go back far enough to reflect the time period with the largest emission reductions. Tørseth et al. (2012) reported average reductions for ambient sulphate and nitrate mass concentrations in Europe of −12% and −1%, respectively, during 2000 to 2009 compared to −24% and −7%, respectively, during 1990 to 2000. These authors also reported statistically significant decreases of the PM_{10} and $PM_{2.5}$ mass concentrations at around 50% of European sites, with total reductions of −18% and −27%, for PM_{10} (24 sites) and $PM_{2.5}$ (13 sites), respectively, during 2000 to 2009. A direct comparison between the stations included in this work and those included in the study of Tørseth et al. (2012) is not possible because of the different timings of the reported σ_{sp} and PM mass concentration measurements. At those stations, where a significant decreasing trend for σ_{sp} is observed and considering a period of 10 years (even if not coincident for all stations), the total reduction for σ_{sp} in Europe is around −35% (cf. Table S8), consistent with the trend reported by Tørseth et al. (2012) for PM in Europe.

Quite good agreement, although again likely biased by the different timings, is also observed when comparing the PM mass concentration and σ_{sp} trends by geographical sector. A significant total reduction of around −40 to −30% was reported for PM_{10} and $PM_{2.5}$ in the Nordic and Baltic sector by Tørseth et al. (2012; cf. Figure 7 in Tørseth et al. (2012)), in close agreement with the statistically significant total decrease of σ_{sp} of around −34% reported for PAL during 2000 to 2010 (cf. Table S8). In the western sector (MHD), the decreasing trend for $PM_{2.5}$ during 2000 to 2009 was insignificant (−10 to 0%) as reported here for σ_{sp} during the period 2001 to 2010. In the central sector, statistically significant decreases for the $PM_{2.5}$ and PM_{10} mass concentrations ranging between −20% and −40% were observed during a 10 year period (2000 to 2009) and the total reduction for σ_{sp} ranged between −38% (HPB) and around −48% (IPR). In the Southwest European sector the total reduction for σ_{sp} is around −32% (at UGR) and −60% (at IZO), whereas Tørseth et al. (2012) reported decreases of around −20 to −40% for the PM_{10} mass concentration in the same geographical sector.

To further confirm the observed close agreement between the PM trends reported in the literature and the trends of σ_{sp} detailed in this work, Table S9 in the Supporting Material reports the comparison between σ_{sp} and PM_{10} and/or $PM_{2.5}$ mass concentration trends calculated at those stations where simultaneous σ_{sp} and PM mass concentration measurements are available. As reported in Table S9, both the observed total reductions and the statistical significance levels of the trends are very similar for σ_{sp} and PM_{10}.

3.6.2 Trends of SAE and BF

The trends for SAE are estimated for three different quantities, namely the SAE is calculated using the three wavelengths (b-g-r), using the blue and the green wavelengths (b-g) and using the green and red wavelengths (g-r). For the periods considered in this work (in bold in Table 2), the SAE calculated using the three wavelengths (b-g-r) shows statistically significant trends at five sites. At PAL (Nordic and Baltic), PUY (Western Europe) and BEO (Eastern Europe) decreasing trends are observed, whereas increasing trends are observed at HPB (Central Europe) and UGR (Southwestern Europe). Uniform negative trends of the columnar Ångström exponent from AERONET data were reported by Li et al. (2014) across Europe and these trends were ascribed to reduced fine-mode anthropogenic emissions. The positive SAE trend observed at HPB and UGR would suggest a shift of the accumulation-mode particles toward smaller sizes and/or a change in the coarse aerosol mode. For example, the SAE increase at UGR might be explained by a progressive relative importance of fine particle emissions driven by a progressive reduction of coarse particles, for example from construction/demolition works due to the economic crisis which affected Spain from 2008 (e.g. Lyamani et al., 2011; Querol et al., 2014; Pandolfi et al., 2016). In fact, Titos et al. (2014) reported a statistically significant decreasing trend for the PM_{10} fraction during the period 2006 to 2010 whereas no trend was observed for the PM_1 fraction. Moreover, at UGR, a statistically significant increasing trend is also observed for the SAE calculated using the green and red wavelengths (g-r), which are likely more sensitive to the coarser particle mode, whereas the trend was non-statistically significant for the SAE at b-g wavelengths.

The possible change in the coarse aerosol mode at UGR is likely also the cause of the observed statistically significant increasing trend of BF (cf. Table 2), given that a positive trend of BF would be consistent with a shift of the accumulation-mode particles toward smaller sizes. Similarly, statistically significant increasing trends for both SAE and BF are also observed at SMR (SAE b-g) and HPB. Statistically significant increasing trends of BF are also observed at the other Nordic and Baltic stations (PAL) and at PUY (Western Europe), where the SAE shows statistically significant decreasing trends, and at IPR (Central Europe) where the trend of SAE is insignificant. Thus, overall, the trends of BF are positive at all stations where BF measurements are available. The opposite sign of the trends for SAE and BF at PAL and PUY could be due to the different effects that the different particle sizes have on SAE and *g* or a progressive change in the mean

diameter of the fine-mode aerosols. Further research involving, for example, size distribution data and a Mie calculation could help in understanding the differences observed in some cases between SAE and BF (or *g*).

Recently, Korras-Carraca et al. (2015) have shown that the column integrated *g* from Modis-Terra showed widely statistically significant positive trends (2002-2010) with stronger increases observed in the eastern and southern Black Sea, as well as over the Baltic and Barents seas. Moreover, both Modis-Terra and Modis-Aqua produce positive trends of *g* in the eastern Mediterranean Sea and the eastern coast of the Iberian Peninsula. Positive trends for *g* correspond to negative trends for BF. The difference observed in our work could be due to the different variability often observed between near-surface measurements and column integrated measurements which can confound the relationship between surface and column optical properties (e.g. Bergin et al., 2000; Lyamani et al., 2010), although it has been shown that a mid-altitude station might be globally representative of the whole atmospheric column (Chauvigne et al., 2016).

3.6.3 Comparison with previous trend analyses

Table 2 shows the comparison, over the same time periods, between the trend analyses performed in this work and the analyses presented by Collaud Coen et al. (2013) for aerosol particle optical properties and by Asmi et al. (2013) for particle number concentrations ($N_{LDL-500}$, N_{20-500} and $N_{100-500}$). An agreement with the results from Collaud Coen et al. (2013) is observed for JFJ, where consistent insignificant trends are detected for the three periods reported in Collaud Coen et al. (2013). For MHD, we observed a non-significant increasing trend for σ_{sp} during 2001 to 2010, whereas Collaud Coen et al. (2013) reported a statistically significant increasing trend for the same period. At PAL, a non-statistically significant trend for σ_{sp} is observed both in the current work and in Collaud-Coen et al. (2013) for the period 2001 to 2010, whereas we observe a statistically significant decreasing trend for the period 2000 to 2010. Moreover, at PAL, we observe a statistically significant decreasing trend for SAE during the two common periods which were insignificant in Collaud Coen et al. (2013). It should be noted that Collaud Coen et al. (2013) reported an insignificant SAE trend at PAL using the Mann-Kendall test whereas they reported statistically significant decreasing trends using the GLS/ARB (generalized least square trends with either autoregressive or block bootstrap confidence intervals) and LMS (least-mean square) methods, consistent with our work. These differences are thus likely due to the relative short period used in these trend analyses and the different sensitivity of the methods used to missing values or the presence of outliers, especially at PAL, where σ_{sp} is very low (cf. Figure 2). For example, in this work, the SAE calculated for PAL during the year 2007 was removed from the trend analysis due to the presence of too many extremely high SAE values, likely explaining the difference observed in SAE compared to the work of Collaud Coen et al. (2013). Moreover, here we use de-seasonalized monthly means for trend analyses whereas Collaud-Coen et al. (2013) used de-

seasonalized medians with a different time granularity (3 days), likely affecting the comparison, especially over relatively short periods.

A comparison of trends analysis results between σ_{sp} and the particle number concentration is not straightforward as the σ_{sp} measurements are more sensitive to the particle number concentration in the upper end of the fine mode than to smaller particles. For example, Asmi et al. (2013) reported that, globally, no strong similarities were observed between σ_{sp} and particle number concentration (N) trends and that the N trends are controlled by particles in the larger range of the Aitken mode and the smaller range of the accumulation mode, i.e. ca. 50–150 nm diameter. In this work, as reported in Table 2, the statistically significant decreasing trend reported for N during the period 2001 to 2010 is not observed for σ_{sp}. However, differences are also observed at PAL between N20 and N100, mainly due to the fact that the DMPS measurements at PAL had long gaps during periods with unusually low concentrations, thus effectively removing low concentrations from the trend analysis (Asmi et al., 2013).

3.6.4 Daytime and night time trend analyses at mountain sites

Finally, the analysis of the trends during daytime (08:00 to 16:00 GMT) and night time (21:00 to 05:00 GMT) by season at the mountain stations are also analysed (Table 3). This analysis could provide information about changes in σ_{sp} during periods when the mountain stations are likely affected by the PBL (e.g. daytime and/or summer) or by the residual layer (e.g. night time in summer) or when the mountain stations are representative of the free troposphere (e.g. night time in winter). Consistent with what is reported in Table 2 for σ_{sp}, the trends are insignificant at JFJ, PUY, CMN and BEO irrespective of the time of the day or season. The decreasing trends observed at HPB, also reported in Table 2, are statistically significant only during autumn, irrespective of the time of day. Conversely, the trend observed for σ_{sp} at IZO reported in Table 2, is not observed on splitting the analysis by time of day and/or season.

Conclusions

This investigation presented the near-surface in situ σ_{sp} (aerosol particle light scattering), SAE (scattering Ångström exponent), BF (backscatter fraction) and *g* (asymmetry parameter) measurements obtained over the past decade at 28 atmospheric observatories which are part of the ACTRIS Research Infrastructure, with most belonging to the GAW network. Results show a large variability of both extensive and intensive aerosol particle optical properties across the network, which is consistent with the previously reported variability observed for other aerosol particle properties such as particle mass concentration, particle number concentration and chemical composition. Main findings can be summarized as follows:

- An increasing gradient of σ_{sp} is observed when moving from remote environments (Arctic/mountain) to regional and to urban environments. At regional level in Europe, σ_{sp} also increases when moving from Nordic and Baltic countries and Western Europe to Central/Eastern Europe whereas no clear spatial gradient is observed for other station environments. For example, the lack of a clear spatial gradient of σ_{sp} measured at mountain observatories is likely due to the different altitudes of the observatories in the different geographical sectors considered in this study. Among the European mountain observatories a relationship was observed between station altitude and the median σ_{sp}, this latter being the highest at the station located at the lower altitude and vice versa.

- Overall, the highest σ_{sp} values are measured at low altitude observatories in Central and Eastern Europe and at some urban observatory in Southern Europe whereas the lowest σ_{sp} values are observed at mountain stations and at Arctic and Antarctic observatories. Low σ_{sp} levels, comparable to those measured at mountain sites, are also observed at the majority of the regional Nordic and Baltic observatories. The σ_{sp} values in Western Europe are on average higher compared to those measured in the Nordic and Baltic regions and lower compared to those measured at a regional level in Southern Europe. Some exceptions to these general features are however observed.

- The SAE does not show any clear gradient as a function of the placement of the station. However, a West to East increasing gradient is observed for both regional and mountain placements suggesting a lower fraction of fine-mode particle in Western/Southwestern Europe compared to Central and Eastern Europe where the fine-mode particles dominate the scattering.

- In fact, in Central and Eastern Europe, independently of the station placement, the SAE is among the highest observed across the network, indicating a large predominance of fine particles. In these regions, the SAE is even higher in summer compared to winter, suggesting the shift toward the small end of the aerosol particle size distribution likely linked to new particle formation events during the warmest months. On average SAE is lower in the Nordic and Baltic and western geographical sectors (likely due to the contribution from coarse-mode sea salt particles), and southern sectors (likely because of the presence of mineral dust particles from African deserts), compared to Central and Eastern Europe.

- The g does not show any clear gradient by station placement or geographical location reflecting the complex relationship of this parameter with the aerosol particles properties such as size distribution, particle shape or refractive index.

- Slightly higher g values are observed in Western Europe compared to Central and Eastern Europe. These differences in the g values, even if small, are consistent with the opposite gradient observed for SAE, this latter being smaller in Western Europe. However, the station-averaged g in Central and Eastern Europe is similar to the mean g observed in the Nordic and Baltic regions and in Southwestern Europe. Thus, contrary to the SAE, a clear relationship between aerosol size and g is not observed.

1   - Seasonal cycles for σ_{sp}, SAE and g are observed in all geographical sectors and explained by

2   different factors. The seasonal cycles are especially marked at a regional level in Central and

3   Eastern Europe where winter time episodes linked with stable air and thermal inversions favour

4   the accumulation of pollutants. In these European regions the SAE (g) is higher (lower) in

5   summer compared to winter due to variations in particle number size distribution due to the

6   enhanced formation of small and optically active particles during new particles formation and

7   subsequent growth. Clear annual cycles are also observed at mountain sites where σ_{sp} is

8   higher in summer because of the enhanced influence of the boundary layer. In some cases, the

9   SAE (g) is also high (low) in summer at mountain sites indicating a higher PBL anthropogenic

10   influence during the warmer months and/or new particles formation episodes. In the Nordic and

11   Baltic regions, the seasonal variation of σ_{sp} is less pronounced compared to Central and

12   Eastern Europe, likely due to the different meteorology and less pronounced PBL variations.

13   Despite the relatively small σ_{sp} seasonal cycles in the Nordic and Baltic regions, SAE (g)

14   increases (decreases) in these regions in summer compared to the winter period likely due to a

15   season-dependent transport of air masses at these remote sites and the enhanced formation of

16   secondary organic aerosols previously observed at these sites during the warmest months. At

17   coastal sites in Northwestern Europe, the presence of sea-salt particles in winter also

18   contributes to the observed pronounced seasonal cycles of SAE and g. in Southern Europe the

19   seasonal cycles are strongly driven by the enhanced formation of secondary sulphate and

20   organic matter in the summer, together with frequent Saharan mineral dust outbreaks.

21   - The analyses of the systematic variabilities of SAE and g as a function aerosol loading (σ_{sp})

22   reveal some common patterns. At all stations, g shows the lowest values at very low σ_{sp} likely

23   because of the formation of new particles in a clean atmosphere followed by

24   condensation/coagulation with, as a consequence, the generation of small but optically active

25   particles. The g value then sharply increases with increasing σ_{sp}, indicating the shift of the

26   particle number size distribution toward the larger end of the accumulation mode. Then, during

27   periods of high σ_{sp} values, the variation of g is less pronounced at the majority of the stations,

28   contrary to the SAE, which increases or decreases, suggesting changes mostly in the coarse

29   aerosol particle mode rather than in the fine mode. At the majority of Northwestern, Central and

30   Eastern European stations, the SAE maintains high values at high σ_{sp} values, indicating that

31   the high σ_{sp} is dominated by fine particles. Conversely, at some sites in Southern Europe the

32   SAE reaches values of around one or lower for high particle loads, indicating that, at these

33   stations, the high σ_{sp} is dominated by mineral dust coarse particles mainly from African

34   deserts. Exceptions are two urban sites in Southwestern Europe where fine particles, probably

35   generated for the most part by traffic (and also from biomass burning) on average dominate the

36   highest measured σ_{sp} values.

- The analyses of the trends reported in this investigation provide evidence that both extensive and intensive aerosol optical properties have significantly changed at some of the locations included here over the last 10 and 15 years. The σ_{sp} decreasing trends reported here are statistically significant at 5 out of 13 stations included in the analyses. These 5 stations are located in the Nordic and Baltic regions, and the central and southwestern sectors. Conversely, σ_{sp} trends which are decreasing are not statistically significant in Western and Eastern Europe. Statistically significant decreasing trends of SAE are observed at 3 out of 10 observatories included in the analysis: one site in the Nordic and Baltic sector and two mountain sites in the western and eastern sectors. These negative trends could be ascribed to reduced fine-mode anthropogenic emissions, as already observed in the literature for columnar SAE in Europe. Conversely, at two stations (one mountain site in Central Europe and one urban site in Southwestern Europe), the SAE shows a statistically significant increasing trend, suggesting a shift in the accumulation-mode particles toward smaller sizes and/or a change in the coarse aerosol mode. At the remaining 5 observatories, the reported SAE trends are not statistically significant. The backscatter fraction shows a statistically significant increasing trend at 5 out of the 9 sites where BF measurements are available. At three stations (the mountain site in Central Europe, the urban site in Southwestern Europe and one of the two sites in the Nordic and Baltic sector), both BF and SAE increase, suggesting consistent evidence of a shift in the accumulation-mode particles toward a smaller size. Conversely, at the other site in the Nordic and Baltic sector and at one mountain site in the western sector the BF increases whereas the SAE decreases.

- A general agreement is observed between the trend analyses preformed in this work and the analyses presented in a previous work confirming the general decreasing trends observed for σ_{sp} in Europe. However, some differences are also observed and likely due to the relative short periods used in these trend analyses and the different sensitivity of the methods used to missing values or presence of outliers. (Mann-Kendall or Theil-Sen vs. GLS/ARB or MLS; means vs. medians; different time granularity)

In conclusion, this investigation provides a clear and useful picture of the spatial and temporal variability of the surface in situ aerosol particle optical properties in Europe. The results presented here give a comprehensive view of the particle optical properties and provide a reliable analysis of aerosol optical parameters for model constraints. In addition, the analyses presented here suggest findings that may need additional investigation. For example, the fact that at some of the stations the trend of σ_{sp} changes in terms of both statistical significance and sign depending on the period used, suggests that trend analyses are necessary in the future when longer-duration records will be available. Moreover, the fact that at some sites BF and SAE show different signs in their trends suggests that further analysis is needed to better understand how other aerosol parameters, such as particle size distribution and mean diameter, affect the relationships between BF and SAE.

Acknowledgments

This project has received funding from the European Union's Horizon 2020 research and innovation programme under grant agreement No 654109, ACTRIS (project No. 262254), ACTRIS-PPP (project No 739530). We also thank the International Foundation High Altitude Research Stations Jungfraujoch and Gornergrat (HFSJG), which made it possible to carry out the experiments at the High Altitude Research Station at the Jungfraujoch and the support of MeteoSwiss within the Swiss program of the Global Atmosphere Watch (GAW) of the WMO. MAD station is co-financed by the PROACLIM (CGL2014-52877-R) project. SMR station acknowledges BACCHUS (project No. 603445), CRAICC (project No. 26060) and Academy of Finland (project No. 3073314). UGR station is co-financed by the Spanish Ministry of Economy and Competitiveness through project CGL2016-81092-R. Measurements at Montseny and Montsec stations were supported by the MINECO (Spanish Ministry of Economy and Competitiveness) and FEDER funds under the PRISMA project (CGL2012-39623-C02/00), by the MAGRAMA (Spanish Ministry of Agriculture, Food and Environment) and by the Generalitat de Catalunya (AGAUR 2014 SGR33 and the DGQA). Measurements at Izaña were supported by the AEROATLAN project (CGL2015-17 66229-P), co-funded by the Ministry of Economy and Competitiveness of Spain and the European Regional Development Fund. Station Košetice is supported by the Ministry of Education, Youth and Sports of the Czech Republic within the project for support of national research infrastructure ACTRIS – participation of the Czech Republic (ACTRIS-CZ – LM2015037). Measurements at Puy de Dôme were partly supported by CNRS-INSU, University Clermont-Auvergne, OPGC and the french CLAP program. PAL station acknowledges KONE Foundation, Academy of Finland (project No. 269095 and No. 296302). CHC station received support from Institut de Recherche pour le Développement (IRD) under both Jeune Equipe program attributed to LFA and support to ACTRIS-FR program. CHC received grants from Labex OSUG@2020 (Investissements d'avenir – ANR10 LABX56). Marco Pandolfi is funded by a Ramón y Cajal Fellowship (RYC-2013-14036) awarded by the Spanish Ministry of Economy and Competitiveness. The authors would like to express their gratitude to D. C. Carslaw and K. Ropkins for providing the OpenAir software used in this paper (Carslaw and Ropkins, 2012; Carslaw, 2012).

Bibliography

Aaltonen, V., Lihavainen, H., Kerminen, V.-M., Komppula, M., Hatakka, J., Eneroth, K., Kulmala, M., and Viisanen, Y.: Measurements of optical properties of atmospheric aerosols in Northern Finland, Atmos. Chem. Phys., 6, 1155-1164, doi:10.5194/acp-6-1155-2006, 2006.

Alastuey, A., Querol, X., Castillo, S., Escudero, M., Avila, A., Cuevas, E., Torres, C., Romero, P.-M., Exposito, F., García, O., Diaz, J. P., Van Dingenen, R., and Putaud, J. P.: Characterisation of TSP and PM2.5 at Izaña and Sta. Cruz de Tenerife (Canary Is lands, Spain) during a Saharan dust episode (July 2002), Atmos. Environ., 39, 4715–4728, doi:10.1016/j.atmosenv.2005.04.018, 2005.

Anderson, T. L. and Ogren, J. A.: Determining Aerosol Radia Radiative Properties Using the TSI 3563 Integrating Nephelometer, Aerosol Sci. Tech., 29, 57–69, 1998.

Andrews, E., Sheridan, P. J., Fiebig, M., McComiskey, A., Ogren, J. A., Arnott, P., Covert, D., Elleman, R., Gasparini, R., Collins, D., Jonsson, H., Schmid, B., and Wang, J.: Comparison of methods for deriving aerosol asymmetry parameter, J. Geophys. Res. Atmos., 111, D05S04, doi:10.1029/2004JD005734, 2006.

Andrews, E., Ogren, J. A., Bonasoni, P., Marinoni, A., Cuevas, E., Rodríguez, S., Sun, J. Y., Jaffe, D. A., Fischer, E. V., Baltensperger, U., Weingartner, E., Collaud Coen, M., Sharma, S., Macdonald, A. M., Leaitch, W. R., Lin, N.-H., Laj, P., Arsov, T., Kalapov, I., Jefferson, A., and Sheridan, P.: Climatology of aerosol radiative properties in the free troposphere, Atmos. Res., 102, 365–393, doi:10.1016/j.atmosres.2011.08.017, 2011.

Asmi, A., Wiedensohler, A., Laj, P., Fjaeraa, A.-M., Sellegri, K., Birmili, W., Weingartner, E., Baltensperger, U., Zdimal, V., Zikova, N., Putaud, J.-P., Marinoni, A., Tunved, P., Hansson, H.-C., Fiebig, M., Kivek¨as, N., Lihavainen, H., Asmi, E., Ulevicius, V., Aalto, P. P., Swietlicki, E., Kristensson, A., Mihalopoulos, N., Kalivitis, N., Kalapov, I., Kiss, G., de Leeuw, G., Henzing, B., Harrison, R. M., Beddows, D., O'Dowd, C., Jennings, S. G., Flentje, H., Weinhold, K., Meinhardt, F., Ries, L., and Kulmala, M.: Number size distributions and seasonality of submicron particles in Europe 2008–2009, Atmos. Chem. Phys., 11, 5505–5538, doi:10.5194/acp-11-5505-2011, 2011.

Asmi, A., Collaud Coen, M., Ogren, J. A., Andrews, E., Sheridan, P., Jefferson, A., Weingartner, E., Baltensperger, U., Bukowiecki, N., Lihavainen, H., Kivek¨as, N., Asmi, E., Aalto, P. P., Kulmala, M., Wiedensohler, A., Birmili, W., Hamed, A., O'Dowd, C., Jennings, S. G., Weller, R., Flentje, H., Mari Fjaeraa, A., Fiebig, M., Lund Myhre, C., Hallar, A. G., Swietlicki, E., Kristensson, A., and Laj, P.: Aerosol decadal trends – Part 2: In-situ aerosol particle number concentrations at GAW and ACTRIS stations, Atmos. Chem. Phys., 13, 895–916, doi:10.5194/acp-13-895-2013, 2013.

Barmpadimos, I., Hueglin, C., Keller, J., Henne, S., and Prevot, A. S. H.: Influence of meteorology on PM10 trends and variability in Switzerland from 1991 to 2008, Atmos. Chem. Phys., 11, 1813– 1835, doi:10.5194/acp-11-1813-2011, 2011.

Barmpadimos, I., Keller, J., Oderbolz, D., Hueglin, C., and Prévôt, A. S. H: One decade of parallel fine (PM2.5) and coarse (PM10–PM2.5) particulate matter measurements in Europe: trends and variability, Atmos. Chem. Phys., 12, 3189-3203, doi:10.5194/acp-12-3189-2012, 2012.

Bergin, M. H., Schwartz, S. E., Halthore, R. N., Ogren, J. A., and Hlavka, D. L.: Comparison of aerosol optical depth inferred from surface measurements with that determined by Sun photometry for cloud-free conditions at a continental US site, J. Geophys. Res., 105, 6807–6816, 2000.

Bond, T. C., Covert, D. S., and Muller, T., Truncation and Angular-Scattering Corrections for Absorbing Aerosol in the TSI 3563 Nephelometer, Aerosol Sci. Tech., 43, 866–871, 2009.

Boulon, J., Sellegri, K., Hervo, M., and Laj, P.: Observations of nucleation of new particles in a volcanic plume, P. Natl. Acad. Sci. USA, 108, 12223–12226, doi:10.1073/pnas.1104923108, 2011.

Bourcier L., K. Sellegri, P. Chausse, J. M. Pichon and P. Laj "Seasonal variation of water-soluble inorganic component in size-segregated aerosol at the puy de Dôme station (1465 m a.s.l.), France", Journal of Atmospheric Chemistry, DOI: 10.1007/s10874-012-9229-2, 2012.

Bukowiecki, N., Weingartner, E., Gysel, M., Collaud Coen, M., Zieger, P., Herrmann, E., Steinbacher, M., Heinz, Gäggeler, W., Baltensperger, U.: A review of more than 20 years of aerosol observation at the high

altitude research station Jungfraujoch, Switzerland (3580 m asl), Aerosol and Air Quality Research, 16: 764–788, doi: 10.4209/aaqr.2015.05.0305, 2016.

Carrico, C.M., Kus, P., Rood, M.J., Quinn, P.K., Bates, T.S.: Mixtures of pollution, dust, sea salt, and volcanic aerosol during ACE-Asia: radiative properties as a function of relative humidity, J. Geophys. Res., 108, doi:10.1029/2003JD003405, 2003.

Carslaw, D. C.: The openair manual – open-source tools for analysing air pollution data, Manual for version 0.7-0, King's College, London, 2012.

Carslaw, D. C. and Ropkins, K.: openair – an R package for air quality data analysis, Environ. Modell. Softw., 27–28, 52–61, 2012.

Cavalli, F., Alastuey, A., Areskoug, H., Ceburnis, D., Cech, J., Genberg, J., Harrison, R.M., Jaffrezo, J.L., Kiss, G., Laj, P., Mihalopoulos, N., Perez, N., Quincey, P., Schwarz, J., Sellegri, K., Spindler, G., Swietlicki, E., Theodosi, C., Yttri, K.E., Aas, W., Putaud, J.P.: European aerosol phenomenology -4: Harmonized concentrations of carbonaceous aerosol at 10 regional background sites across Europe, Atmos. Environ.,144, 133-145, 2016.

Chauvigné A., K. Sellegri, M. Hervo, N. Montoux, P. Freville, and Goloub, P.: Comparison of the aerosol optical properties and size disribution retrieved by Sun photometer with in-situ measurements at mid-latitude, Atmos. Meas. Tech., 9, 4569-4585, doi:10.5194/amt-9-4569-2016, 2016.

Colette, A., Aas, W., Banin, L., Braban, C., Ferm, M., González Ortiz, A., Ilyin, I., Mar, K., Pandolfi, M., Putaud, J.-P., Shatalov, V., Solberg, S., Spindler, G., Tarasova, O., Vana, M., Adani, M., Almodovar, P., Berton, E., Bessagnet, B., Bohlin-Nizzetto, P., Boruvkova, J., Breivik, K., Briganti, G., Cappelletti, A., Cuvelier, K., Derwent, R., D'Isidoro, M., Fagerli, H., Funk, C., Garcia Vivanco, M., González Ortiz, A., Haeuber, R., Hueglin, C., Jenkins, S., Kerr, J., de Leeuw, F., Lynch, J., Manders, A., Mircea, M., Pay, M., Pritula, D., Putaud, J.-P., Querol, X., Raffort, V., Reiss, I., Roustan, Y., Sauvage, S., Scavo, K., Simpson, D., Smith, R., Tang, Y., Theobald, M., Tørseth, K., Tsyro, S., van Pul, A., Vidic, S., Wallasch, M., and Wind, P.: Air Pollution trends in the EMEP region between 1990 and 2012., Tech. Rep. Joint Report of the EMEP Task Force on Measurements and Modelling (TFMM), Chemical Co-ordinating Centre (CCC), Meteorological Synthesizing Centre- East (MSC-E), Meteorological Synthesizing Centre-West (MSC-W) EMEP/CCC Report 1/2016, Norwegian Institute for Air Research, Kjeller, Norway, URL http://www. unece.org/fileadmin/DAM/env/documents/2016/AIR/Publications/ Air_pollution_trends_in_the_EMEP_region.pdf, 2016., 2016.

Collaud Coen, M., Weingartner, E., Nyeki, S., Cozic, J., Henning, S., Verheggen, B., Gehrig, R., and Baltensperger, U.,: Long-term trend analysis of aerosol variables at the highalpine site Jungfraujoch, J. Geophys. Res., 112, D13213, doi:10.1029/2006JD007995, 2007.

Collaud Coen, M., Weingartner, E., Apituley, A., Ceburnis, D., Fierz-Schmidhauser, R., Flentje, H., Henzing, J. S., Jennings, S. G., Moerman, M., Petzold, A., Schmid, O., and Baltensperger, U.: Minimizing light absorption measurement artifacts of the Aethalometer: evaluation of five correction algorithms, Atmos. Meas. Tech., 3, 457–474, doi:10.5194/amt-3-457-2010, 2010.

Collaud Coen, M., Andrews, E., Asmi, A., Baltensperger, U., Bukowiecki, N., Day, D., Fiebig, M., Fjaeraa, A. M., Flentje, H., Hyvärinen, A., Jefferson, A., Jennings, S. G., Kouvarakis, G., Lihavainen, H., Lund Myhre, C., Malm, W. C., Mihapopoulos, N., Molenar, J. V., O'Dowd, C., Ogren, J. A., Schichtel, B. A., Sheridan, P., Virkkula, A., Weingartner, E., Weller, R., and Laj, P.: Aerosol decadal trends – Part 1: In-situ optical measurements at GAW and IMPROVE stations, Atmos. Chem. Phys., 13, 869-894, doi:10.5194/acp-13-869-2013, 2013.

Collaud Coen, M., Andrews, E., Aliaga, D., Andrade, M., Angelov, H., Bukowiecki, N., Ealo, M., Fialho, P., Flentje, H., Gannet Hallar, A., Hooda, R., Kalapov, I., Krejci, R., Lin, N-H., Marinoni, A., Ming, J., Nguyen, N. A., Pandolfi, M., Pont, V., Ries, L., Rodríguez, S., Schauer, G., Sellegri, K., Sharma, S., Sun, J., Tunved, P., Velasquez, P., and Ruffieux, D.: The topography contribution to the influence of the atmospheric boundary layer at high altitude stations, submitted to Atm. Chem. Phys. Discuss., July 2017.

Crumeyrolle, S., Manninen, H. E., Sellegri, K., Roberts, G., Gomes, L., Kulmala, M., Weigel, R., Laj, P., and Schwarzenboeck, A.: New particle formation events measured on board the ATR-42 aircraft during the EUCAARI campaign, Atmos. Chem. Phys., 10, 6721–6735, doi:10.5194/acp-10-6721-2010, 2010.

Cusack, M., Alastuey, A., Pérez, N., Pey, J., and Querol, X.: Trends of particulate matter (PM2:5) and chemical composition at a regional background site in the Western Mediterranean over the last nine years (2002–2010), Atmos. Chem. Phys., 12, 8341–8357, doi:10.5194/acp-12-8341-2012, 2012.

Delene, D. J. and Ogren, J. A.: Variability of aerosol optical properties at four North American surface monitoring sites, J. Atmos. Sci., 59, 1135–1149, 2002.

Eleftheriadis, K., Ochsenkuhn, K.M., Lymperopoulou, T., Karanasiou, A., Razos, P., Ochsenkuhn-Petropoulou, M.: Influence of local and regional sources on the observed spatial and temporal variability of size resolved atmospheric aerosol mass concentrations and water-soluble species in the Athens metropolitan area, Atm. Environ., 97, 252-261, http://dx.doi.org/10.1016/j.atmosenv.2014.08.013, 2014.

Diaz, A.M., Diaz, J.P., Exposito, F.J., Hernandez-Leal, P.A., Savoie, D., Querol, X.: Air masses and aerosols chemical components in the free troposphere at the subtropical northeast Atlantic region, J. Atmos. Chem., 53, 63–90, 2006.

Diapouli, E., Manousakas, M. I., Vratolis, S., Vasilatou, V., Pateraki, S.,Bairachtari, K. A., Querol, X., Amato, F., Alastuey, A., Karanasiou, A. A., Lucarelli, F., Nava, S., Calzolai, G., Gianelle, V. L., Colombi, C., Alves, C., Custo´dio, D., Pio, C., Spyrou, C., Kallos, G. B., Eleftheriadis, K.: AIRUSE-LIFE +: estimation of natural source contributions to urban ambient air PM10 and PM2:5 concentrations in southern Europe – implications to compliance with limit values. Atmos. Chem. Phys., 17, 3673–3685, 2017..

Doherty, S.J., Quinn, P.K., Jefferson, A., Carrico, C.M., Anderson, T.L., Hegg, D.: A comparison and summary of aerosol optical properties as observed in situ from aircraft, ship, and land during ACE-Asia, J. Geophys. Res., 110, D04201. doi:10.1029/2004JD004964, 2005.

Ealo, M., Alastuey, A., Ripoll, A., Pérez, N., Minguillón, M. C., Querol, X., and Pandolfi, M.: Detection of Saharan dust and biomass burning events using near-real-time intensive aerosol optical properties in the north-western Mediterranean, Atmos. Chem. Phys., 16, 12567-12586, https://doi.org/10.5194/acp-16-12567-2016, 2016.

EEA: European Environmental Agency Air quality in Europe – 2013 report, EEA report 9/2013, Copenhagen, 1725–9177, available at: http://www.eea.europa.eu/publications/air-quality-in-europe-2013, 2013.

EEA: European Environmental Agency Air quality in Europe – 2016 report, EEA Report No 28/2016, Copenhagen, available at: file:///D:/Usuari/Descargas/Air%20quality%20in%20Europe%202016%20report%20THAL16027ENN%20(1). pdf, 2016.

EMEP, Transboundary particulate matter in Europe Status report 2008 NILU Reference: O-98134. Edited by Yttri, K.-E., Aas, W., Tørseth, K., Stebel, K., Nyíri, Á., Tsyro, S., Merckova, K., Wankmüller, R., Winiwarter, W., Bauer, H., Caseiro, A., Puxbaum, H., Holzer-Popp, T., Schroedter-Homscheidt, M. (http://tarantula.nilu.no/projects/ccc/reports/emep4-2008.pdf), 2008.

Engvall, A.-C., Krejci, R., Ström, J., Treffeisen, R., Scheele, R., Hermansen, O., and Paatero, J.: Changes in aerosol properties during spring-summer period in the Arctic troposphere, Atmos. Chem. Phys., 8, 445-462, https://doi.org/10.5194/acp-8-445-2008, 2008.

EPA: Emissions of primary particulate matter and secondary particulate matter precursors, Assessment published December 2011, available at: http://www.epa.gov/ttn/chief/trends/, CSI 003, 2011.

Esteve, A.R., Estellés, V., Utrillas, M.P., Martínez-Lozano, J.A.: In-situ integrating nephelometer measurements of the scattering properties of atmospheric aerosols at an urban coastal site in western Mediterranean, Atm. Env., 47, 43-50, 2012.

Fierz-Schmidhauser, R., Zieger, P., Vaishya, A., Monahan, C., Bialek, J., O'Dowd, C. D., Jennings, S. G., Baltensperger, U., Weingartner, E.: Light scattering enhancement factors in the marine boundary layer (Mace Head, Ireland), J. Geophys. Res., 115, D20204, doi:10.1029/2009JD013755, 2010a.

Fierz-Schmidhauser, R., Zieger, P., Gysel, M., Kammermann, L., DeCarlo, P. F., Baltensperger, U., and Weingartner, E.: Measured and predicted aerosol light scattering enhancement factors at the high alpine site Jungfraujoch, Atmos. Chem. Phys., 10, 2319–2333, doi:10.5194/acp-10-2319-2010, 2010b.

Guerreiro, C., Leeuw, F. de, Foltescu, V., Horálek, J., and European Environment Agency: Air quality in Europe 2014 report, Luxembourg: Publications Office, available at: http://bookshop.europa.eu/uri?target=EUB:NOTICE:THAL14005:EN:HTML (last access: 2 June 2016), 2014.

Hansen, J.E. and Travis, L.D.: Light scattering in the planetary atmosphere, Space Science Reviews, 16 527-610, 1974.

Henschel, S., Querol, X., Atkinson, R., Pandolfi, M., Zeca, A., Le Tertre, A., Analitis, A., Katsouyanni, K., Chanel, O., Pascal, M., Bouland, C., Haluza, D., Medina, S., and Goodman, P. G.: Ambient air SO2 patterns in 6 European cities, Atmos. Environ., 79, 236–247, 2013.

Hollander, M., and Wolfe, D. A.: Nonparametric statistical methods, 2nd ed. Wiley, New York, New York, 787, 1999.

IPCC: Climate Change 2014: Synthesis Report. Contribution of Working Groups I, II and III to the Fifth Assessment Report of the Intergovernmental Panel on Climate Change [Core Writing Team, R.K. Pachauri and L.A. Meyer (eds.)]. IPCC, Geneva, Switzerland, 151 pp, 2014.

Kalivitis, N., Bougiatioti, A., Kouvarakis, G., Mihalopoulos, N.: Long term measurements of atmospheric aerosol optical properties in the Eastern Mediterranean, Atmosp. Res., 102, 351–357, 2011.

Karanasiou, A., Querol, X., Alastuey, A., Perez, N., Pey, J., Perrino, C., Berti, G., Gandini, M., Poluzzi, V., Ferrari, S., de la Rosa, J.: Particulate matter and gaseous pollutants in the Mediterranean Basin: Results from the MED-PARTICLES project, Sci. of Tot. Environ., 488–489, 297–315, 2014.

Kecorius, S., Kivekäs, N., Kristensson, A., Tuch, T., Covert, D.S., Birmili, W., Lihavainen, H., Hyvärinen, A.P., Martinsson, J., Sporre, M.K., Swietlicki, E., Wiedensohler, A. Ulevicius, V.: Significant increase of aerosol number concentrations in air masses crossing a densely trafficked sea area, Oceanologia, 58, 1—12, 2016.

Korras-Carraca, M. B., Hatzianastassiou, N., Matsoukas, C., Gkikas, A., and Papadimas, C. D.: The regime of aerosol asymmetry parameter over Europe, the Mediterranean and the Middle East based on MODIS satellite data: evaluation against surface AERONET measurements, Atmos. Chem. Phys., 15, 13113-13132, doi:10.5194/acp-15-13113-2015, 2015.

Laj, P., Klausen, J., Bilde, M., Plaß-Duelmer, C., Pappalardo, G., Clerbaux, C, Baltensperger, U., Hjorth, J., Simpson, D., Reimann, S., Coheur, P.-F., Richter, A., De Mazie, M., Rudich, Y., McFiggans, G., Torseth, K., Wiedensohler, A., Morin, S., Schulz, M., Allan, J. D., Attie, J.-L., Barnes, I., Birmili, W., Cammas, J. P., Dommen, J., Dorn, H.-P., Fowler, D., Fuzzi, S., Glasius, M., Granier, C., Hermann, M., Isaksen, I. S. A., Kinne, S., Koren, I., Madonna, F., Maione, M., Massling, A., Moehler, O., Mona, L., Monks, P. S., Müller , D., Müller , T., Orphal, J., Peuch, V.-H., Stratmann, F., Tanre, D., Tyn dall, F., Abo Riziqmm, A., Van Roozendael, M., Villani P., Wehner, B., Wex, H., and Zardini, A. A.: Measuring atmospheric composition change, Atmos. Environ, 43, 5351–5414, doi:10.1016/j.atmosenv.2009.08.020, 2009.

Li, J., Carlson, B. E., Dubovik, O., and Lacis, A. A.: Recent trends in aerosol optical properties derived from AERONET measurements, Atmos. Chem. Phys., 14, 12271–12289, doi:10.5194/acp-14-12271-2014, 2014.

Lihavainen, H., Hyvärinen, A., Asmi, E., Hatakka, J. and Viisanen, Y.: Long-term variability of aerosol optical properties in northern Finland, Boreal Environment Research, 20, 526–541, 2015a.

Lihavainen, H., Asmi, E., Aaltonen, V., Makkonen, U. and Kerminen, V-M.: Direct radiative feedback due to biogenic secondary organic aerosol estimated from boreal forest site observations, Environ. Res. Lett., 10, doi:10.1088/1748-9326/10/10/104005, 2015b.

Lyamani, H., Olmo, F. J., and Alados-Arboledas, L.: Physical and optical properties of aerosols over an urban location in Spain: seasonal and diurnal variability, Atmos. Chem. Phys., 10, 239-254, doi:10.5194/acp-10-239-2010, 2010.

Lyamani, H., Olmo, F.J., Foyo, I., Alados-Arboledas, L.: Black carbon aerosols over an urban area in south-eastern Spain: Changes detected after the 2008 economic crisis, Atmos. Environ., 45, 6423–6432, 2011.

Lyamani, H., Fernández-Gálvez, J., Pérez-Ramírez, D., Valenzuela, A., Antón, M., Alados, I., Titos, G., Olmo, F.J., Alados-Arboledas, L.: Aerosol properties over two urban sites in South Spain during an extended stagnation episode in winter season, Atmos. Environ., 62, 424-432, 2012.

Ma, N., Birmili, W., Müller, T., Tuch, T., Cheng, Y. F., Xu, W. Y., Zhao, C. S., and Wiedensohler, A.: Tropospheric aerosol scattering and absorption over central Europe: a closure study for the dry particle state, Atmos. Chem. Phys., 14, 6241-6259, doi:10.5194/acp-14-6241-2014, 2014.

Manktelow, P. T., Mann, G. W., Carslaw, K. S., Spracklen, D. V., and Chipperfield, M. P.: Regional and global trends in sulphate aerosol since the 1980's, Geophys. Res. Lett., 34, L14803, doi:10.1029/2006GL028668, 2007.

Marenco, F., Bonasoni, P., Calzolari, F., Ceriani, M., Chiari, M., Cristofanelli, P., D'Alessandro, A., Fermo, P., Lucarelli, F., Mazzei, F., Nava, S., Piazzalunga, A., Prati, P., Valli, G., and Vecchi, R.: Characterization of atmospheric aerosols at Monte Cimone, Italy, during summer 2004: Source apportionment and transport mechanisms, J. Geoph. Res., 111, doi:10.1029/2006JD007145, 2006.

Marshall, S.F., Covert, D.S., and Charlson, R.J.: Relationship between asymmetry parameter and hemispheric backscatter ratio: implications for climate forcing by aerosols, App. Opt., 34, 27, 6306 – 6311, 1995.

Molnár, A., Bécsi, Z., Imre, K., Gácser, V.,Zita Ferenczi, Z.: Characterization of background aerosol properties during a wintertime smog episode, Aerosol and Air Quality Research, 16, 1793–1804, 2016.

Müller, T., Nowak, A., Weidensohler, A., Sheridan, P., Laborde, M., Covert, D.S., Marinoni, A., Imre, K., Henzing, B., Roger, J.-C., Martins dos Santos, S., Wilhelm, R.,Wang, Y.-Q., de Leeuw, G.: Angular illumination and truncation of three different integrating nephelometers: implications for empirical size-based corrections, Aerosol Sci. Technol., 43, 581–586, 2009.

Müller, T., Laborde, M., Kassell, G., and Wiedensohler, A.: Design and performance of a three-wavelength LED-based total scatter and backscatter integrating nephelometer, Atmos. Meas. Tech., 4, 1291-1303, https://doi.org/10.5194/amt-4-1291-2011, 2011.

Nyeki, S., Baltensperger, U., Colbeck, I., Jost, D.T., Weingartner, E., Gäggeler, H.W.: The Jungfraujoch high-alpine research station (3454 m) as a background continental site for the measurement of aerosol parameters, J. Geophys. Res., 103, 6097-6107, 1998.

Nyeki, S., Halios, C.H., Baum, W., Eleftheriadis, K., Flentje, H., Gröbner, J., Vuilleumier, L., and Wehrli, C.: Ground-based aerosol optical depth trends at three high-altitude sites in Switzerland and southern Germany from 1995 to 2010, J. Geophys. Res., 117, D18202, doi:10.1029/2012JD017493, 2012.

Obiso, V., and Jorba, O.: Impact of aerosol physical properties on atmospheric radiative e ects due to aerosol-radiation interaction, Sci. Tot. Environ., 112, 68-82, 2017.

O'Connor, T.C., Jennings, S.G., O'Dowd, C.D.: Highlights of fifty years of atmospheric aerosol research at Mace Head, Atmos. Res., 90, 338–355, 2008.

Ogren, J. A., Andrews, E., McComiskey, A., Sheridan, P., Jefferson, A., and Fiebig, M.: New insights into aerosol asymmetry parameter, in: Proceedings of the 16th ARM Science Team Meeting, Albuquerque, NM, USA, 2006.

Pandolfi, M., Cusack, M., Alastuey, A., and Querol, X.: Variability of aerosol optical properties in the Western Mediterranean Basin, Atmos. Chem. Phys., 11, 8189–8203, doi:10.5194/acp-11-8189-2011, 2011.

Pandolfi, M., Ripoll, A., Querol, X., and Alastuey, A.: Climatology of aerosol optical properties and black carbon mass absorption cross section at a remote high-altitude site in the western Mediterranean Basin, Atmos. Chem. Phys., 14, 6443-6460, doi:10.5194/acp-14-6443-2014, 2014.

Pandolfi, M., Querol, X., Alastuey, A., Jimenez, J. L., Jorba, O., Day, D., Ortega, A., Cubison, M. J., Comerón, A., Sicard, M., Mohr, C., Prévôt, A. S. H., Minguillón, M. C., Pey, J., Baldasano, J. M., Burkhart, J. F., Seco, R., Peñuelas, J., van Drooge, B. L., Artiñano, B., Di Marco, C., Nemitz, E., Schallhart, S., Metzger, A., Hansel, A., Lorente, J., Ng, S., Jayne, J., and Szidat, S.: Effects of sources and meteorology on particulate matter in the Western Mediterranean Basin: An overview of the DAURE campaign, J. Geophys. Res.-Atmos., 119, 4978–5010, doi:10.1002/2013JD021079, 2014a.

Pandolfi, M., Alastuey, A., Pérez, N., Reche, C., Castro, I., Shatalov, V., and Querol, X.: Trends analysis of PM source contributions and chemical tracers in NE Spain during 2004–2014: a multi-exponential approach, Atmos. Chem. Phys., 16, 11787-11805, doi:10.5194/acp-16-11787-2016, 2016.

Pey, J., Querol, X., Alastuey, A., Forastiere, F., and Stafoggia, M.: African dust outbreaks over the Mediterranean Basin during 2001–2011: PM10 concentrations, phenomenology and trends, and its relation with synoptic and mesoscale meteorology, Atmos. Chem. Phys., 13, 1395–1410, doi:10.5194/acp-13-1395-2013, 2013.

Putaud, J.P., Raes, F., Van Dingenen, R., Brüggemann, E., Facchini, M.C., Decesari, S., Fuzzi, S., Gehrig, R., Hüglin, C., Laj, P., Lorbeer, G., Maenhaut, W., Mihalopoulos, N., Müller, K., Querol, X., Rodriguez, S., Schneider, J., Spindler, G., Ten Brink, H., Tørseth, K., Alfred Wiedensohler, A.: European aerosol phenomenology d2: chemical characteristics of particulate matter at kerbside, urban, rural and background sites in Europe, Atmos. Environ., 38, 2579-2595, 2004.

Putaud, J.P., Van Dingenen, R., Alastuey, A., Bauer, H., Birmili,W., Cyrys, J., Flentje, H., Fuzzi, S., Gehrig, R., Hansson, H.C., Harrison, R.M., Hermann, H., Hitzenberger, R., Hüglin, C., Jones, A.M., Kasper-Giebl, A., Kiss, G., Kousa, A., Kuhlbusch, T.A.J., L€oschau, G., Maenhaut, W., Molnar, A., Moreno, T., Pekkanen, J., Perrino, C., Pitz, M., Puxbaum, H., Querol, X., Rodriguez, S., Salma, I., Schwarz, J., Smolik, J., Schneider, J., Spindler, G., ten Brink, H., Tursic, J., Viana, M., Wiedensohler, A., Raes, F.: A European aerosol phenomenology d 3: physical and chemical characteristics of particulate matter from 60 rural, urban, and kerbside sites across Europe, Atmos. Environ., 44, 1308-1320, 2010.

Putaud, J. P., Cavalli, F., Martins dos Santos, S., and Dell'Acqua, A.: Long-term trends in aerosol optical characteristics in the Po Valley, Italy, Atmos. Chem. Phys., 14, 9129-9136, doi:10.5194/acp-14-9129-2014, 2014.

Querol, X., Pey, J., Pandolfi, M., Alastuey, A., Cusack, M., Perez, N., Moreno, T., Viana, M., Mihalopoulos, N., Kallos, G., and Kleanthous, S.: African dust contributions to mean ambient PM10 mass-levels across the Mediterranean Basin, Atmos. Environ., 43, 4266–4277, doi:10.1016/j.atmosenv.2009.06.013, 2009.

Querol, X., , Alastuey, A., Pandolfi, M., Reche, C., Pérez, N., Minguillón, M. C., Moreno, T., Viana, M., Escudero, M., Orio, A., Pallarés, M., and Reina, F.: 2001–2012 trends on air quality in Spain, Sci. Total Environ., 490, 957–969, doi:10.1016/j.scitotenv.2014.05.074, 2014.

Revuelta, M.A., Artiñano, B., Gómez-Moreno, F.J., Viana, M., Reche, C., Querol, X., Fernández, A.J., Mosquera, J.L., Núñez, L., Pujadas, M., Herranz, A., López, B., Molero, F., Bezares, J.C., Coz, E., Palacios, M., Sastre, M., Férnandez, J.M., Salvador, P., Aceña, B.: Ammonia levels in different kinds of sampling sites in the central Iberian Peninsula, Proceedings of the 2nd Iberian meeting on aerosol science and technology, RICTA 2014.

Ripoll, A., Pey, J., Minguillón, M. C., Pérez, N., Pandolfi, M., Querol, X., and Alastuey, A.: Three years of aerosol mass, black carbon and particle number concentrations at Montsec (southern Pyrenees, 1570 m a.s.l.), Atmos. Chem. Phys., 14, 4279-4295, https://doi.org/10.5194/acp-14-4279-2014, 2014.

Rodríguez, S., Alastuey, A., Alonso-Pérez, S., Querol, X., Cuevas, E., Abreu-Afonso, J., Viana, M., Pérez, N., Pandolfi, M., and de la Rosa, J.: Transport of desert dust mixed with North African industrial pollutants in the subtropical Saharan Air Layer, Atmos. Chem. Phys., 11, 6663-6685, doi:10.5194/acp-11-6663-2011, 2011.

Rodríguez, S., Cuevas, E., Prospero, J. M., Alastuey, A., Querol, X., López-Solano, J., García, M. I., and Alonso-Pérez, S.: Modulation of Saharan dust export by the North African dipole, Atmos. Chem. Phys., 15, 7471-7486, https://doi.org/10.5194/acp-15-7471-2015, 2015.

Rose C., K. Sellegri, Fernando Velarde, Isabel Moreno, Kay Weinhold, Ali Wiedensholer, and Laj, P.: Frequent nucleation events at the high altitude station of Chacaltaya (5240 m a.s.l.), Bolivia, Atmos. Environ., 102, 18-29, doi :10.1016/j.atmosenv.2014.11.015, 2015.

Rotstayn, L. D., Collier, M. A., Chrastansky, A., Jeffrey, S. J., and Luo, J.-J.: Projected effects of declining aerosols in RCP4.5: unmasking global warming?, Atmos. Chem. Phys., 13, 10883-10905, doi:10.5194/acp-13-10883-2013, 2013.

Sherman, J. P., Sheridan, P. J., Ogren, J. A., Andrews, E., Hageman, D., Schmeisser, L., Jefferson, A., and Sharma, S.: A multi-year study of lower tropospheric aerosol variability and systematic relationships from four North American regions, Atmos. Chem. Phys., 15, 12487-12517, https://doi.org/10.5194/acp-15-12487-2015, 2015.

Schuster, G. L., Dubovik, O., and Holben, B. N.: Angstrom exponent and bimodal aerosol size distributions, J. Geophys. Res., 111, D07207, doi:101029/2005JD006328, 2006.

Seinfeld, J. H. and Pandis, S. N.: Atmospheric Chemistry and Physics, John Wiley and Sons, New York, 1998.

Sen, P. K.: Estimates of regression coefficient based on Kendall's tau, J. Am. Stat. Assoc., 63, 1379–1389, 1968.

Spindler, G., Bruggemann, E., Gnauk, T., Gruner, Müller , A. K., Herrmann, H.: A four-year size-segregated characterization study of particles PM10, PM2.5 and PM1 depending on air mass origin at Melpitz, Atmos. Environ.,44, 164-173, 2010.

Stohl, A., Aamaas, B., Amann, M., Baker, L. H., Bellouin, N., Berntsen, T. K., Boucher, O., Cherian, R., Collins, W., Daskalakis, N., Dusinska, M., Eckhardt, S., Fuglestvedt, J. S., Harju, M., Heyes, C., Hodnebrog, Ø., Hao, J., Im, U., Kanakidou, M., Klimont, Z., Kupiainen, K., Law, K. S., Lund, M. T., Maas, R., MacIntosh, C. R., Myhre, G., Myriokefalitakis, S., Olivié, D., Quaas, J., Quennehen, B., Raut, J.-C., Rumbold, S. T., Samset, B. H., Schulz, M., Seland, Ø., Shine, K. P., Skeie, R. B., Wang, S., Yttri, K. E., and Zhu, T.: Evaluating the climate and air quality impacts of short-lived pollutants, Atmos. Chem. Phys., 15, 10529-10566, doi:10.5194/acp-15-10529-2015, 2015.

Ström, J., Umegård, J., Torseth, K., Tunved, P., Hansson, H. C., Holmen, K., Wismann, V., Herber, A., and Konig-Langlo, G.: One year of particle size distribution and aerosol chemical composition measurements at the Zeppelin Station, Svalbard, March 2000-March 2001, Phys. Chem. Earth, 28, 1181–1190, 2003.

Theil, H.: A rank invariant method of linear and polynomial regression analysis, I, II, III, Proceedings of the Koninklijke Nederlandse Akademie Wetenschappen, Series A, Mathematical Sciences, 386–392, 521–525, 1397–1412, 1950.

Titos, G., Foyo-Moreno, I., Lyamani, H., Querol, X., Alastuey, A., Alados-Arboledas, L.: Optical properties and chemical composition of aerosol particles at an urban location: An estimation of the aerosol mass scattering and absorption efficiencies, J. Geophys. Res. Atm., 117, 4, D04206, 2012.

Titos, G., Lyamani, H., Pandolfi, M., Alastuey, A., Alados-Arboledas, L.: Identification of fine (PM1) and coarse (PM10-1) sources of particulate matter in an urban environment, Atmos. Environ., 89, 593-602, 2014.

Titos, G., del Águila, A., Cazorla, A., Lyamani, H., Casquero-Vera, J.A., Colombi, C., Cuccia, E., Gianelle, V., Močnik, G., Alastuey, A., Olmo, F.J., Alados-Arboledas, L.: Spatial and temporal variability of carbonaceous aerosols: Assessing the impact of biomass burning in the urban environment, Sci. of Tot. Environ., 578, 613-625, 2017.

Tørseth, K., Aas, W., Breivik, K., Fjæraa, A. M., Fiebig, M., Hjellbrekke, A. G., Lund Myhre, C., Solberg, S., and Yttri, K. E.: Introduction to the European Monitoring and Evaluation Programme (EMEP) and observed atmospheric composition change during 1972–2009, Atmos. Chem. Phys., 12, 5447–5481, doi:10.5194/acp-12-5447-2012, 2012.

Tunved,P., Hansson, H.-C., Kerminen, V.-M., Ström, J., Dal Maso, M., Lihavainen, H., Viisanen, Y., Aalto, P. P., Komppula, M., Kulmala, M.: High Natural Aerosol Loading over Boreal Forests, Science, 312, 5771, 261-263, DOI: 10.1126/science.1123052, 2006.

Valenzuela, A., Olmo, F.J., Lyamani, H., Antón, M., Titos, G., Cazorla, A., Alados-Arboledas, L.: Aerosol scattering and absorption Angström exponents as indicators of dust and dust-free days over Granada (Spain), Atmos. Res., 154, 1-13, 2015.

Van Dingenen, R., Putaud, J.P., Raes, F., Baltensperger, U., Charron, A., Facchini, M.C., Decesari, S., Fuzzi, S., Gehrig, R., Hansson, H.C., Harrison, R.M., Hüglin, C., Jones, A.M., Laj, P., Lorbeer, G., Maenhaut, W., Palgren, F., Querol, X., Rodriguez, S., Schneider, J., Ten Brink, H., Tunved, P., Tørseth, K., Wehner, B., Weingartner, E., Wiedensohler, A., Wåhlin, P.: A European aerosol phenomenology_1: physical characteristics of particulate matter at kerbside, urban, rural and background sites in Europe, Atmos. Environ., 38, 2561-2577, 2004.

van Donkelaar, A., Randall, M., Brauer, M., Kahn, R., Levy, R., Verduzco, C., and Villeneuve, P. J. Global estimates of exposure to fine particulate matter concentrations from satellite-based aerosol optical depth, Environ. Health Persp., 118, 847–855, doi:10.1289/ehp.0901623, 2010.

Venzac, H., Sellegri, K., Villani, P., Picard, D., and Laj, P.: Seasonal variation of aerosol size distributions in the free troposphere and residual layer at the puy de Dome station, France, Atmos. Chem. Phys., 9, 1465–1478, doi:10.5194/acp-9-1465-2009, 2009.

Virkkula, A., Backman, J., Aalto, P. P., Hulkkonen, M., Riuttanen, L., Nieminen, T., dal Maso, M., Sogacheva, L., de Leeuw, G., and Kulmala, M.: Seasonal cycle, size dependencies, and source analyses of aerosol optical properties at the SMEAR II measurement station in Hyytiälä, Finland, Atmos. Chem. Phys., 11, 4445–4468, doi:10.5194/acp-11-4445-2011, 2011.

Vrekoussis, M., Liakakou, E., Koc-ak, M., Kubilay, N., Oikonomou,1, K., Sciare, J., Mihalopoulos, N.: Seasonal variability of optical properties of aerosols in the Eastern Mediterranean, Atmosp. Environ., 39, 7083–7094, 2005.

WMO/GAW report 227: Aerosol Measurement Procedures, Guidelines and Recommendations, 2nd Edition, 2016, 103 pp. August 2016 (WMO-No. 1177).

Zanatta, M., Gysel, M., Bukowiecki, N., Müller, T., Weingartner, E., Areskoug, H., Fiebig, M., Yttri, K.E., Mihalopoulos, N., Kouvarakis, G., Beddows, D., Harrison, R.M., Cavalli, F., Putaud, J.P., Spindler, G., Wiedensohler, A., Alastuey, A., Pandolfi, M., Sellegri, K., Swietlicki, E., Jaffrezo, J.L., Baltensperger, U., Laj, P.: A European aerosol phenomenology-5: Climatology of black carbon optical properties at 9 regional background sites across Europe, Atm. Env., 145, 346-364, 2016.

Zieger, P., Fierz-Schmidhauser, R., Gysel, M., Ström, J., Henne, S., Yttri, K. E., Baltensperger, U., and Weingartner, E.: Effects of relative humidity on aerosol light scattering in the Arctic, Atmos. Chem. Phys., 10, 3875–3890, doi:10.5194/acp-10-3875-2010, 2010.

Zieger, P., Kienast-Sjögren, E., Starace, M., von Bismarck, J., Bukowiecki, N., Baltensperger, U., Wienhold, F. G., Peter, T., Ruhtz, T., Collaud Coen, M., Vuilleumier, L., Maier, O., Emili, E., Popp, C., and Weingartner, E.: Spatial variation of aerosol optical properties around the high-alpine site Jungfraujoch (3580 m a.s.l.), Atmos. Chem. Phys., 12, 7231-7249, doi:10.5194/acp-12-7231-2012, 2012.

Zieger, P., Fierz-Schmidhauser, R., Poulain, L., Müller, T., Birmili, W., Spindler, G., Wiedensohler, A., Baltensperger, U. and Weingartner, E.: Influence of water uptake on the aerosol particle light scattering coefficients of the Central European aerosol, Tellus B: Chemical and Physical Meteorology, 66:1, 22716, DOI: 10.3402/ tellusb.v66.22716, 2014.

Zieger, P., Väisänen, O., Corbin, J.C., Partridge, D.G., Bastelberger, S., Mousavi-Fard, M., Rosati, B., Gysel, M., Krieger, U.K., Leck, C., Nenes, A., Riipinen, I., Virtanen, A., and Salter, M.E.: Revising the hygroscopicity of inorganic sea salt particles, Nature Communication, DOI: 10.1038/ncomms15883, 2017.

1 **Tables**

3 **Table 1:** List of ACTRIS observatories providing aerosol particle scattering measurements

Observatory name/setting (1)	Country	Observatory code	Lat, Long	Altitude [m a.s.l.]	Geographical location	Inlet	Nephelometer model	Period (a)
Arctic observatories								
Zeppelin **(ZEP)**	Svalbard (Norway)	NO0042G	78.9067 N, 11.8883 E	474	Nordic and Baltic	PM_{10}	TSI3563	07/2010 −12/2014
Pallas **(PAL)**	Finland	FI0096G	67.97 N, 24.12 E	565	Nordic and Baltic	PM_5; $PM_{2.5}$; PM_{10} (b)	TSI3563	02/2000 −12/2015
Antarctic observatories								
Troll **(TRL)**	Antarctica	NO0058G	-72.0167 N, 2.5333 E	1309	Antarctica	whole air; PM_{10} (c)	TSI3563	02/2007 −12/2015
Mountain observatories								
Puy de Dome **(PUY)**	France	FR0030R	45.7667 N, 2.95 E	1465	West	whole air	TSI3563	01/2007 −12/2014
Izaña **(IZO)**	Spain	ES0018G	28.309 N, -16.4994 E	2373	Southwest	PM_{10}	TSI3563	03/2008 − 12/2015
Montsec **(MSA)**	Spain	ES0022R	42.0513 N, 0.44 E	1570	Southwest	$PM_{2.5}$; PM_{10} (d)	ECOTECH Aurora3000	01/2013 − 12/2015
Jungfraujoch **(JFJ)**	Switzerland	CH0001G	46.5475 N, 7.985 E	3578	Central	whole air	TSI3563	07/1995 −12/2015
Mt. Cimone **(CMN)**	Italy	IT0009R	44.1833 N, 10.7 E	2165	Central	whole air	ECOTECH Aurora M9003; TSI 3563 (e)	05/2007 −12/2015
Hohenpeissenberg **(HPB)**	Germany	DE0043G	47.8 N, 11.0167 E	985	Central	PM_{10}	TSI3563	01/2006 −12/2015
Beo Moussala **(BEO)**	Bulgaria	BG0001R	42.1667 N, 23.5833 E	2971	East	whole air	TSI3563	03/2007 −12/2015
Mt. Chacaltaya **(CHC)**	Bolivia	BO0001R	-16.2000 N, -68.09999 E	5240	South America	whole air	ECOTECH Aurora3000	01/2012 − 12/2015 (f)
Coastal observatories								
Preila **(PLA)**	Lithuania	LT0015R	55.35 N, 21.0667 E	5	Nordic and Baltic	PM_{10}	TSI3563	12/2012 −04/2014
Mace Head **(MHD)**	Ireland	IE0031R	53.3258 N, -9.8994 E	5	West	whole air	TSI3563	07/2001 −12/2013
Finokalia **(FKL)** (2)	Greece	GR0002R	35.3167 N, 25.6667 E	250	Southeast	whole air; PM_1; PM_{10} (g)	RR M903; Ecotech Aurora1000 (h)	04/2004 −12/2015
Regional/rural observatories								
Birkenes II **(BIR)**	Norway	NO0002R	58.3885 N, 8.252 E	219	Nordic and Baltic	PM_{10}	TSI3563	07/2009 −12/2015
Hyytiälä **(SMR)**	Finland	FI0050R	61.85N, 24.2833 E	181	Nordic and Baltic	PM_{10}	TSI3563	05/2006 −12/2015
Vavihill **(VHL)** (3)	Sweden	SE0011R	56.0167 N, 13.15 E	175	Nordic and Baltic	PM_{10}	ECOTECH Aurora3000	03/2008 −04/2014
Observatory Perenne **(OPE)**	France	FR0022R	48.5622 N, 5.505555 E	392	West	whole air; PM_{10} (i)	ECOTECH Aurora3000	09/2012 −12/2015
Cabauw **(CBW)** (4)	The Netherlands	NL0011R	51.9703 N, 4.9264 E	1	West	PM_{10}	TSI3563	01/2008 −12/2012
Montseny **(MSY)**	Spain	ES1778R	41.7667 N, 2.35 E	700	Southwest	PM_{10}	ECOTECH Aurora3000	01/2010 −12/2015
Košetice **(KOS)**	Czech Republic	CZ0007R	49.58333N, 15.0833 E	534	Central	PM_{10}	TSI3563	03/2013 − 12/2015
Melpitz **(MPZ)** (5)	Germany	DE0044R	51.53 N, 12.93 E	86	Central	PM_{10}	TSI3563	01/2007 −12/2015
Ispra **(IPR)**	Italy	IT0004R	45.8 N, 8.6333 E	209	Central	PM_{10}	TSI3563	01/2004 −12/2014
K-Puszta **(KPS)**	Hungary	HU0002R	46.9667 N, 19.5833 E	125	East	PM_1; PM_{10} (j)	TSI3563	05/2006 −12/2014

Urban/sub-urban observatories								
SIRTA (SIR)	France	FR0020R	48.7086 N, 2.1589 E	162	West	PM_1	ECOTECH M9003	07/2012 –12/2013
Madrid (MAD)	Spain	ES1778R	40.4627 N, -3.717 E	669	Southwest	$PM_{2.5}$; PM_{10} (k)	ECOTECH Aurora3000	01/2014 – 12/2014
Granada (UGR)	Spain	ES0020U	37.164 N, -3.605 E	680	Southwest	whole air	TSI3563	01/2006 –12/2015
Athens (DEM)	Greece	GR0100B	37.9905 N, 23.8095 E	270	Southeast	PM_{10}	ECOTECH Aurora3000	01/2012 –12/2015

(1) Observatory codes from EBAS; (2) GAW code: FIK; (3) GAW code: VAV; (4) GAW code: CES; (5) GAW code: MEL; (a) start-end of measurements; total aerosol particle scattering was used as reference for measurement period; (b) PM_5 (2000-08/2005), $PM_{2.5}$ (08/2005-2007) and PM_{10} (2008-2015); (c) whole air (2007-2009) and PM_{10} (2010-2015); (d) $PM_{2.5}$ (2013-03/2014) and PM_{10} (04/2014-2015); (e) ECOTECH Aurora M9003 during 2007-2013 and TSI 3563 (2014-2015); (f) only measurements performed during the year 2012 were used in this investigation; (g) whole air (2004-2008), PM_{10} (2009-2011), PM_1 (2011-2012), PM_{10} (2013-2015); (h) RR M903 during 2004-2011, Ecotech AURORA1000 during 2012-2015; (i) whole air (2012-08/2013) and PM_{10} (09/2014-2015); (j) PM_1 (2006-04/2008) and PM_{10} (05/2008-2014); (k) PM_{10} from 03/2014.

Table 2: Trends of aerosol particle scattering coefficient (σ_{sp}), scattering Ångström exponent (SAE) and backscatter fraction (BF). Three trends for SAE are reported: SAE calculated as a linear fit using; three wavelengths (b-g-r), using the blue and green wavelengths (b-g) and using the green and red wavelengths (g-r). Trend results are reported for the whole period available at each station until 2015 (bold) and for the periods reported in Collaud Coen et al. (2013) and Asmi et al. (2013). Trends are considered as statistically significant for a p-value of <0.05. Statistically significant increasing or decreasing trends are highlighted with up (⬆) and down (⬇) red and green arrows, respectively. Non-statistically significant increasing or decreasing trends are highlighted with up (↑) and down (↓) grey arrows, respectively. Grey coloured table cells highlight stations included in this work but not included in the works of Collaud Coen et al. (2013) or Asmi et al. (2013). $: parameters removed in this work and in the work of Collaud Coen et al. (2013) because of measurement gaps, low data coverage or break points for one or more wavelengths. #: Only available for 2014-2015; ± not available.

Legend: ⬆ = red up (significant increase); ⬇ = green down (significant decrease); ↑ = grey up (non-significant increase); ↓ = grey down (non-significant decrease); ↔ = no change.

Station	period	Trend (This work) σsp	SAE b-g-r	SAE b-g	SAE g-r	BF	MK Trend (Collaud Coen et al., 2013) σsp	SAE b-r	SAE b-g	SAE g-r	BF	MK Trend (Asmi et al., 2013) Particle number N	N20 (20-500 nm)	N100 (100-500 nm)
Nordic and Baltic														
PAL	**2000 - 2015**	↑	⬇	↓	⬇	⬆								
	2000 - 2010	⬇	⬇	$	$	↑	↓	↑	$	$	↑			
	2001 - 2010	↓	⬇	$	$	↑	↓	↑	$	$	↑	↓ (10-500 nm)	↔	⬆
	1996 - 2010											↓ (10-500 nm)		
SMR	**2006 - 2015**	⬇	↑	⬆	↑	⬆								
	1996 - 2011												⬇	⬇
	2001 - 2010												⬇	⬇
Western														
MHD	**2001 - 2013**	↓	$	$	$	$								
	2000 - 2010											⬇ (3-500 nm)		
	2001 - 2010	↑	$	$	$	$	⬆	$	$	$	$	↑ (3-500 nm)		
PUY	**2007 - 2014**	↓	⬇	⬇	⬇	⬆								
Central														
HPB	**2006 - 2015**	⬇	⬆	⬆	↑	⬆								
	2001 - 2010						↑	$	$	$	$			
	2002 - 2010						↓	$	$	$	$			
	1995 - 2011											↑ (15-500 nm)		
IPR [1]	**2004 - 2014**	⬇	↑	↑	↑	⬆								
MPZ	**2007 - 2015**	↓	↓	↓	↓	↑								
	1997 – 1998 and 2004 - 2010												↑	↑
JFJ	**1995 - 2015**	↓	$	$	$	$								
	1995 - 2010	↑	$	$	$	$	↑	$	$	$	$			
	1996 - 2010	↑	$	$	$	$	↑	$	$	$	$			
	2001 - 2010	↓	$	$	$	$	↓	$	$	$	$	⬇ (10-500 nm)		
	1997 - 2010	↑	$	$	$	$						↑ (10-500 nm)		
CMN	**2007 - 2015**	↓	#	#	#	#								
Eastern														
BEO	**2007 - 2015**	↓	⬇	⬇	⬇	↓								

		SCATTERING					
Station	**period**	daytime		nighttime		24h	
		Sp	Su	Sp	Su	Sp	Su
		Au	Wi	Au	Wi	Au	Wi
KPS	**2006 - 2014**	↑	↓	↓ (green)	↑	↑	

Southwestern

Station	period						
IZO	**2008 - 2015**	↓ (green)	↑	↑	↑	$	
UGR	**2006 - 2015**	↓ (green)	↑ (red)	↑	↑ (red)	↑ (red)	

(1)   A statistically significant decreasing trend of σ_{sp} at IPR was also reported by Putaud et al. (2014) for the period 2002 – 2010.

Table 3: Daytime (08:00 to 16:00 GMT) and night time (21:00 to 05:00 GMT) σ_{sp} trends by season calculated for the periods considered in this work. Sp: Spring; Su: Summer; Au: Autumn; Wi: Winter. Trends are considered as statistically significant at a p-value of <0.05. Statistically significant increasing or decreasing trends are highlighted with up (↑) and down (↓) red and green arrows, respectively. Non-statistically significant increasing or decreasing trends are highlighted with up (↑) and down (↓) grey arrows, respectively.

Station	**period**	SCATTERING					
		daytime		nighttime		24h	
		Sp	Su	Sp	Su	Sp	Su
		Au	Wi	Au	Wi	Au	Wi
JFJ	1995 - 2015	↓	↓	↓	↓	↓	↓
		↑	↓	↑	↓	↑	↓
HPB	2006 - 2015	↓	↓	↓	↓	↓	↓
		↓ (green)	↓	↓ (green)	↓	↓ (green)	↓
PUY	2006 - 2014	↓	↓	↓	↓	↓	↓
		↓	↓	↓	↓	↓	↓
CMN	2007 - 2015	↓	↑	↓	↓	↓	↓
		↓	↓	↓	↓	↓	↓
BEO	2007 - 2015	↓	↓	↓	↑	↓	↓
		↓	↓	↓	↑	↓	↑
IZO	2008 - 2015	↓	↓	↓	↓	↓	↓
		↑	↓	↑	↓	↑	↓

1 **Figures**
2
3
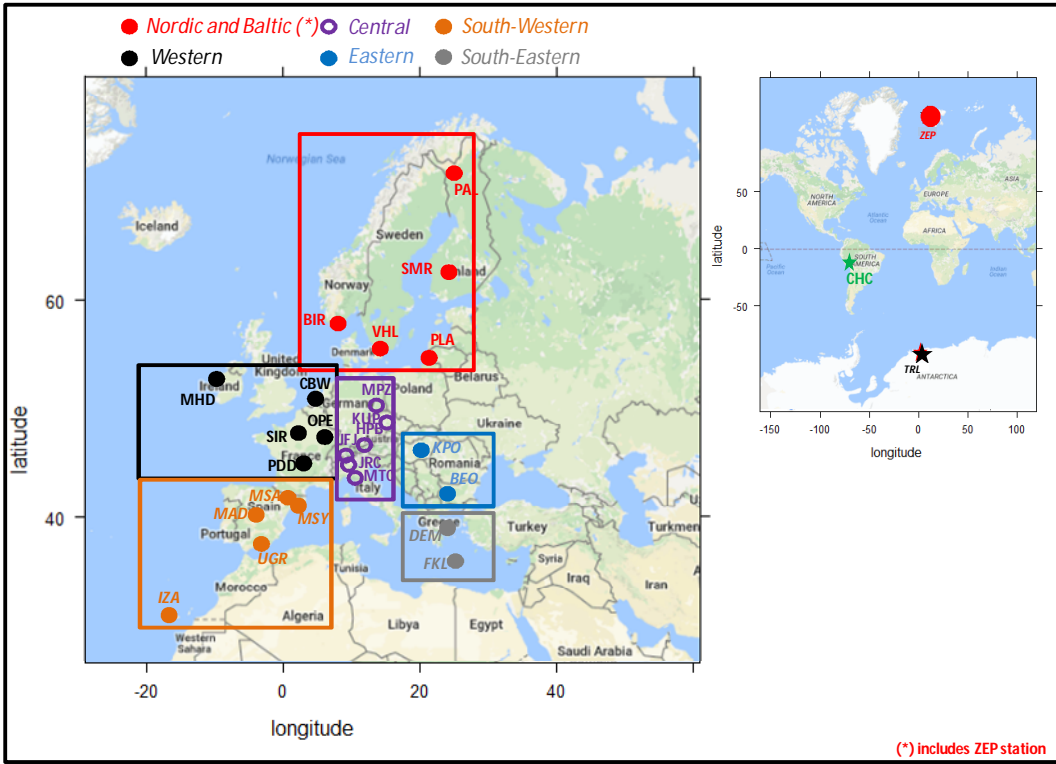
6 **Figure 1:** Locations of the 28 ACTRIS stations included in this work.
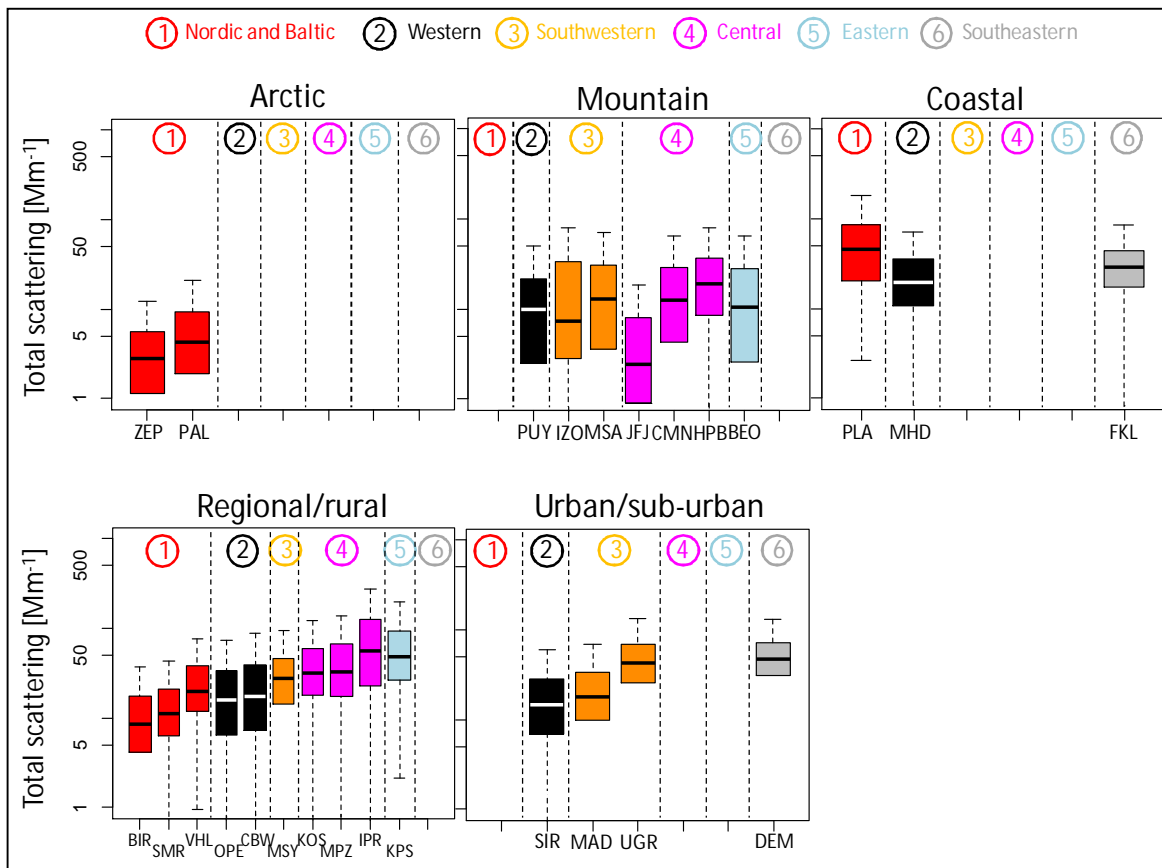
Figure 2: Total aerosol scattering coefficients in the green divided by station setting. Different colours highlight different geographical locations. At SIR, aerosol scattering was available only at 450 nm. Medians (horizontal lines in the boxes), percentiles 25 and 75 (lower and upper limits of the boxes, respectively) and percentiles 5 and 95 (lower and upper limits of the vertical dashed lines) are reported. Hourly data were used for the statistics.
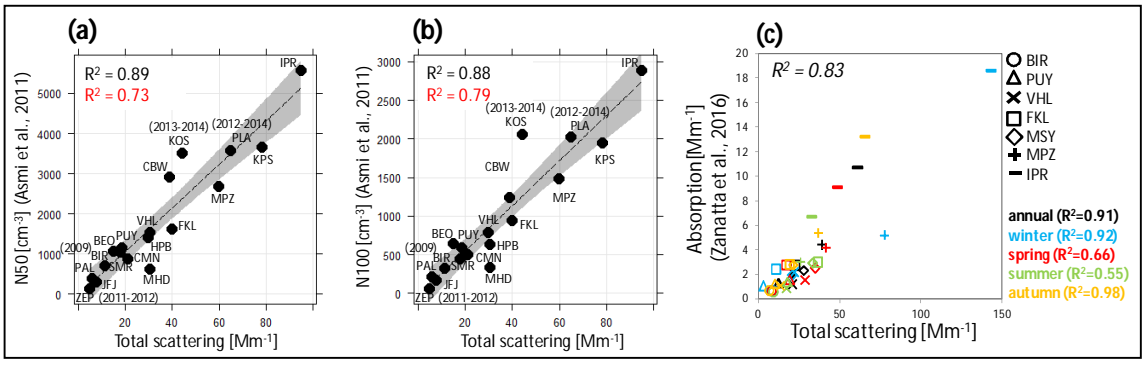
Figure 3: Relationship between: (a) N50 (mean particle number concentration between 50 nm and 500 nm), (b) N100 (mean particle number concentration between 100 nm and 500 nm), (c) absorption coefficient and mean aerosol particle total scattering coefficient. (a) and (b): data averaged over the period 2008 to 2009. For ZEP, BIR, KOS and PLA aerosol particle scattering measurements were not available during 2008 to 2009 and different periods were used. R^2 values, highlighted in red, were obtained using the median values. (c) Data averaged as in Zanatta et al. (2016).
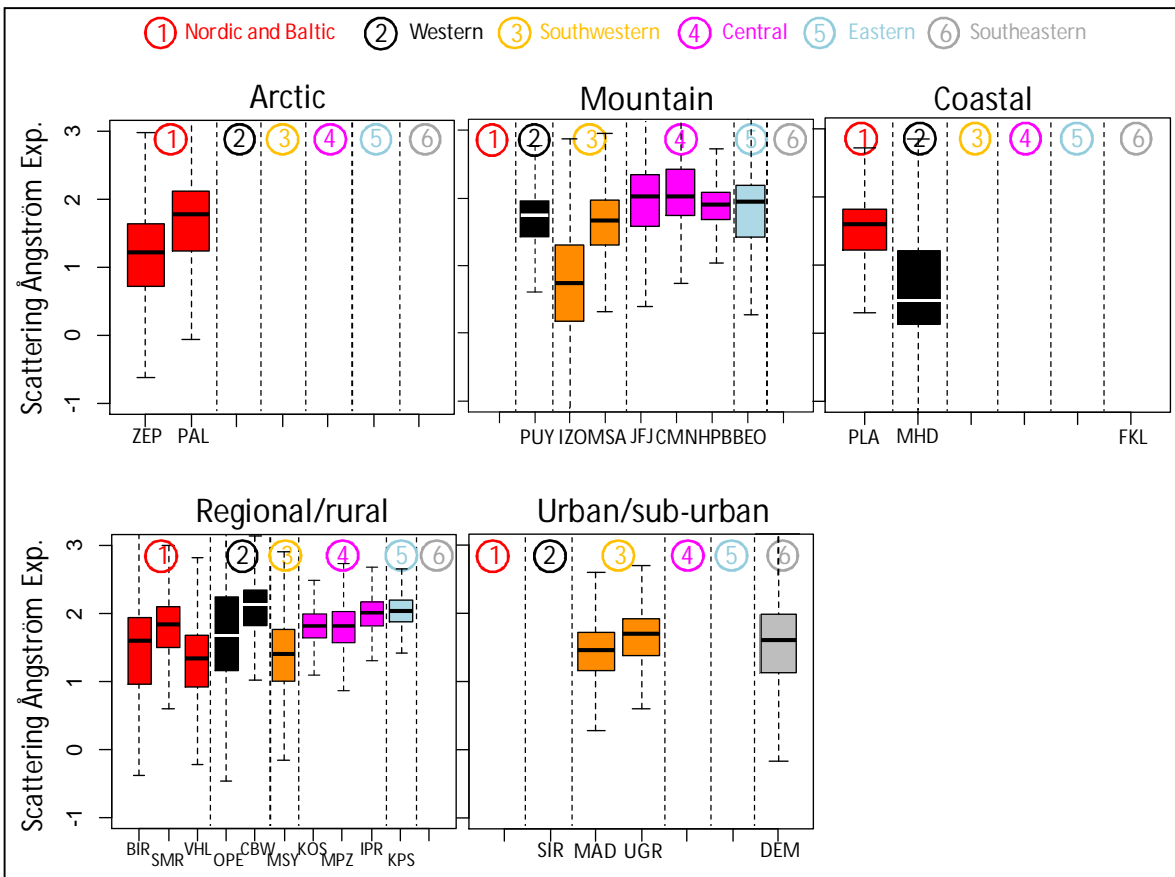
Figure 4: Scattering Ångström exponent divided by station setting. Different colours highlight different geographical locations. Medians (horizontal lines in the boxes), percentiles 25 and 75 (lower and upper limits of the boxes, respectively) and percentiles 5 and 95 (lower and upper limits of the vertical dashed lines) are reported. Hourly data were used for the statistics.

2
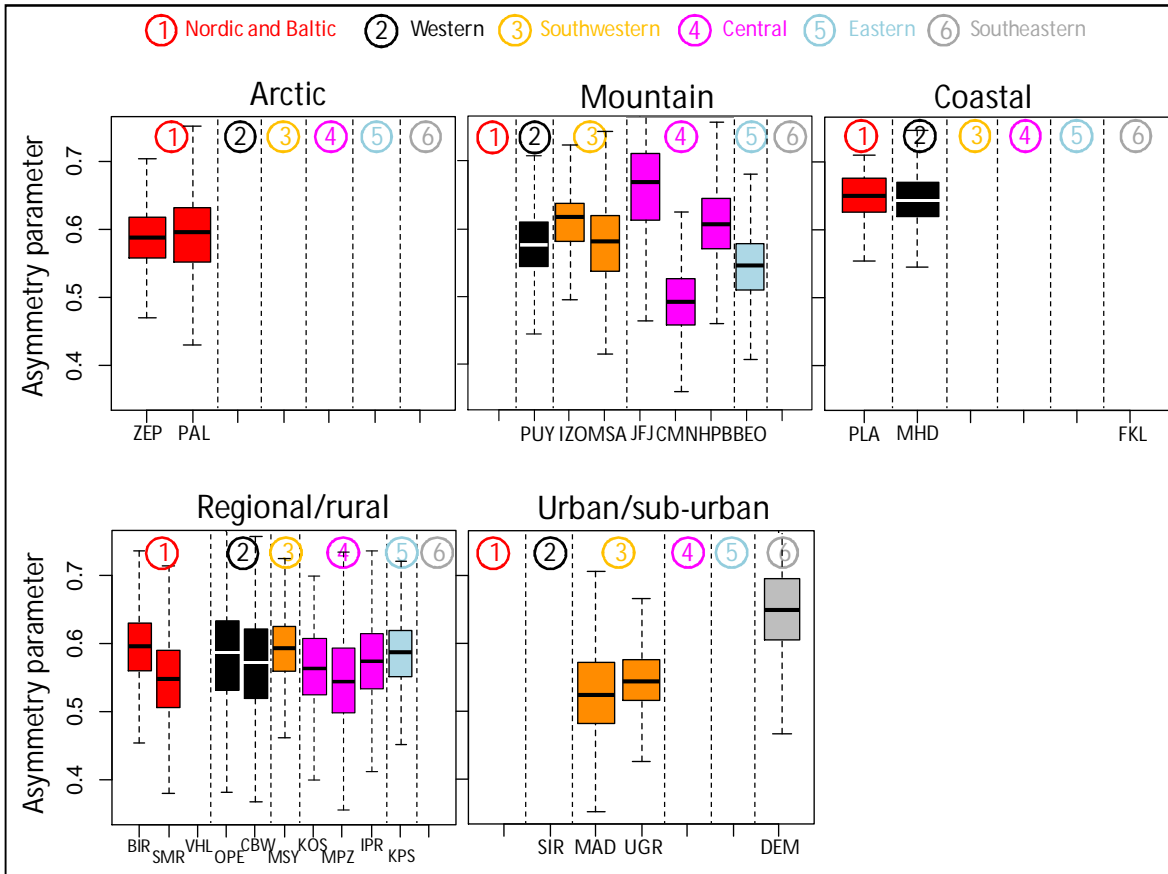
Figure 5: Asymmetry parameter in the green divided by station setting. Different colours highlight different geographical locations. Medians (horizontal lines in the boxes), percentiles 25 and 75 (lower and upper limits of the boxes, respectively) and percentiles 5 and 95 (lower and upper limits of the vertical dashed lines) are reported. Hourly data were used for the statistics.

5
6
7
8
9
10
11
12
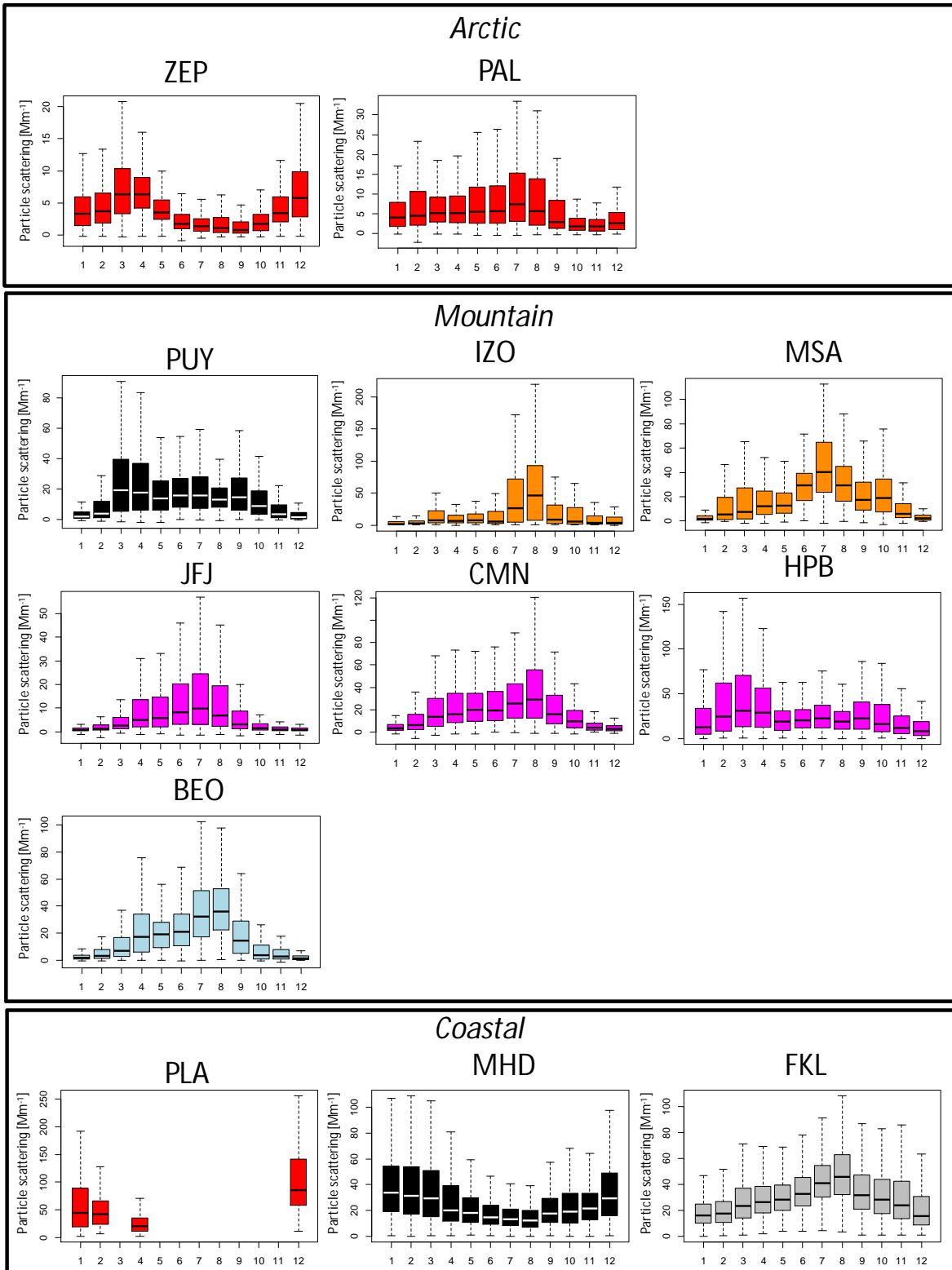
Figure 6: Seasonal cycles of σ_{sp} [Mm^{-1}] measured in the green nephelometer wavelength.
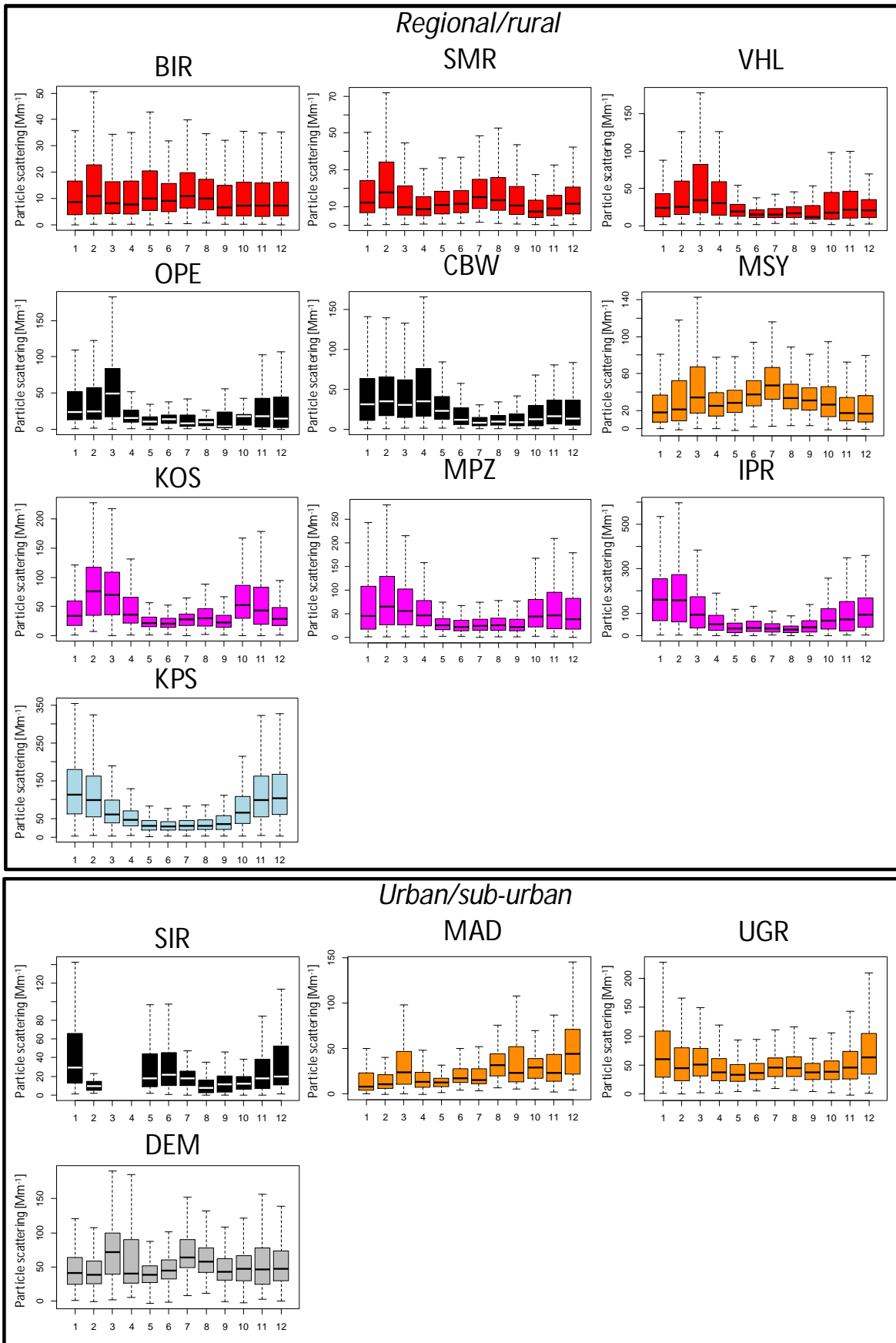
Figure 6: (Continued) Seasonal cycles of σ_{sp} [Mm^{-1}] measured in the green nephelometer wavelength.
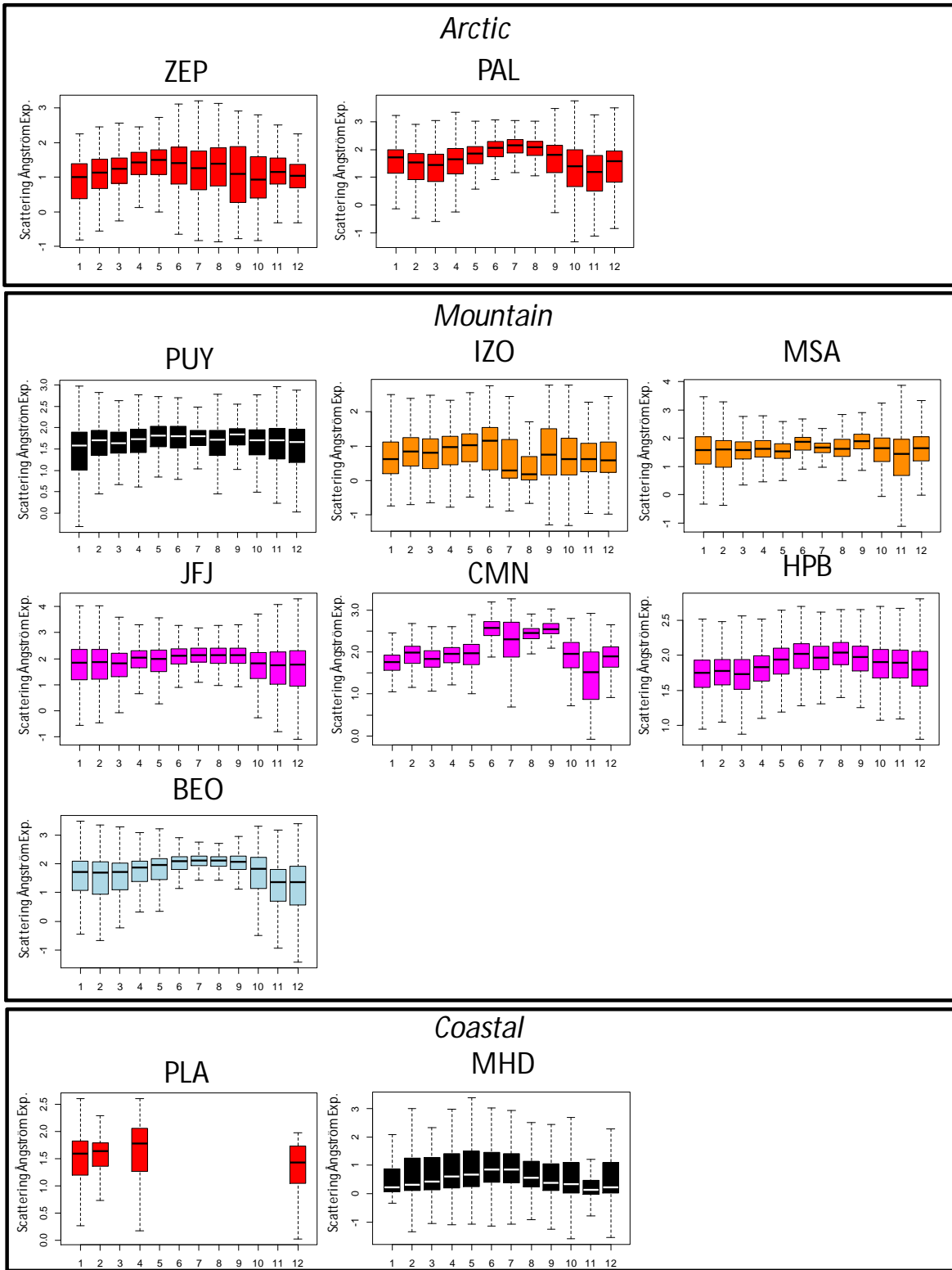
Figure 7: Seasonal cycles of SAE (calculated using the three nephelometer wavelengths).
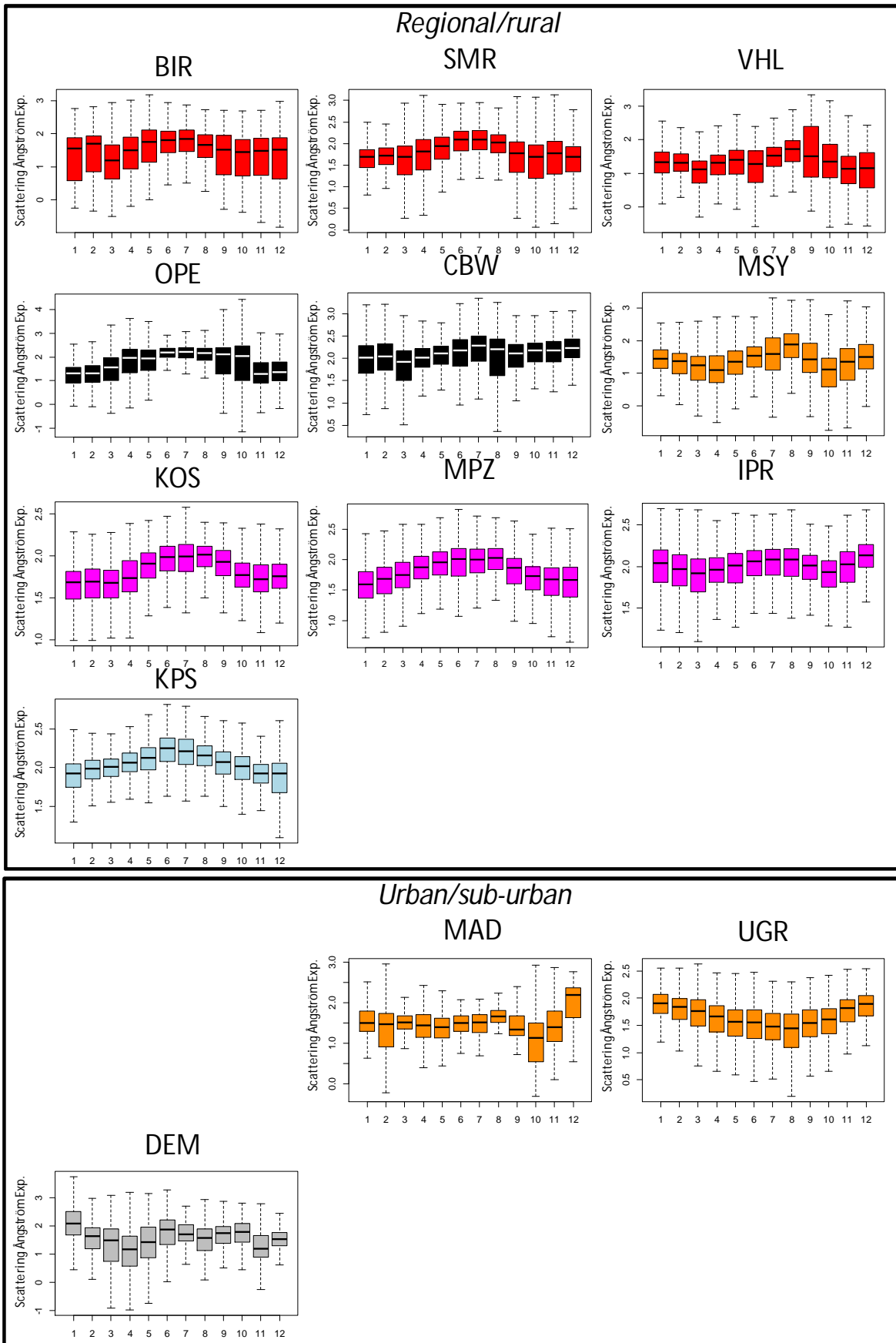
Figure 7: (Continued) Seasonal cycles of SAE (calculated using the three nephelometer wavelengths).
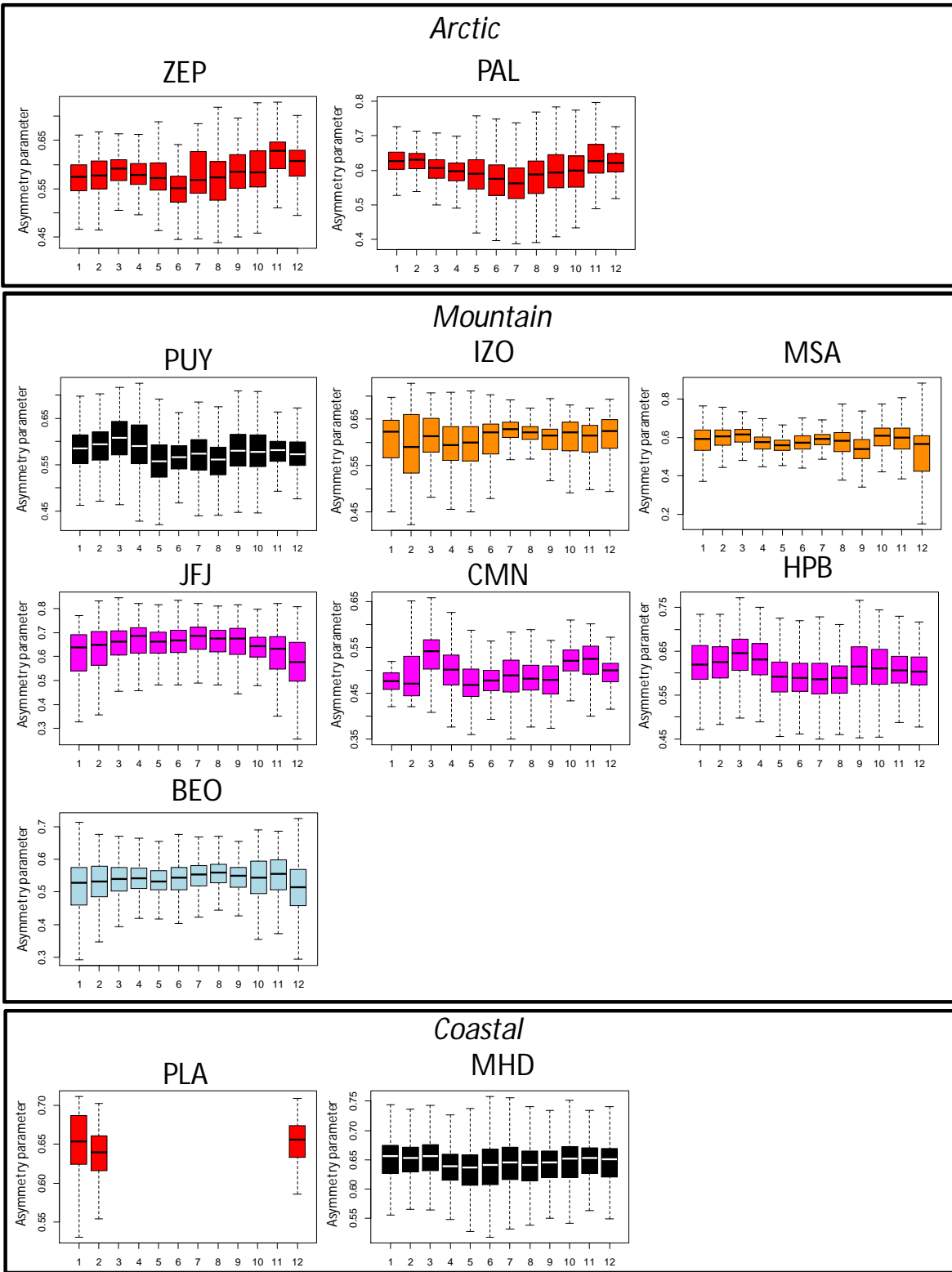
Figure 8: Seasonal cycles of *g* (calculated for the green wavelength).
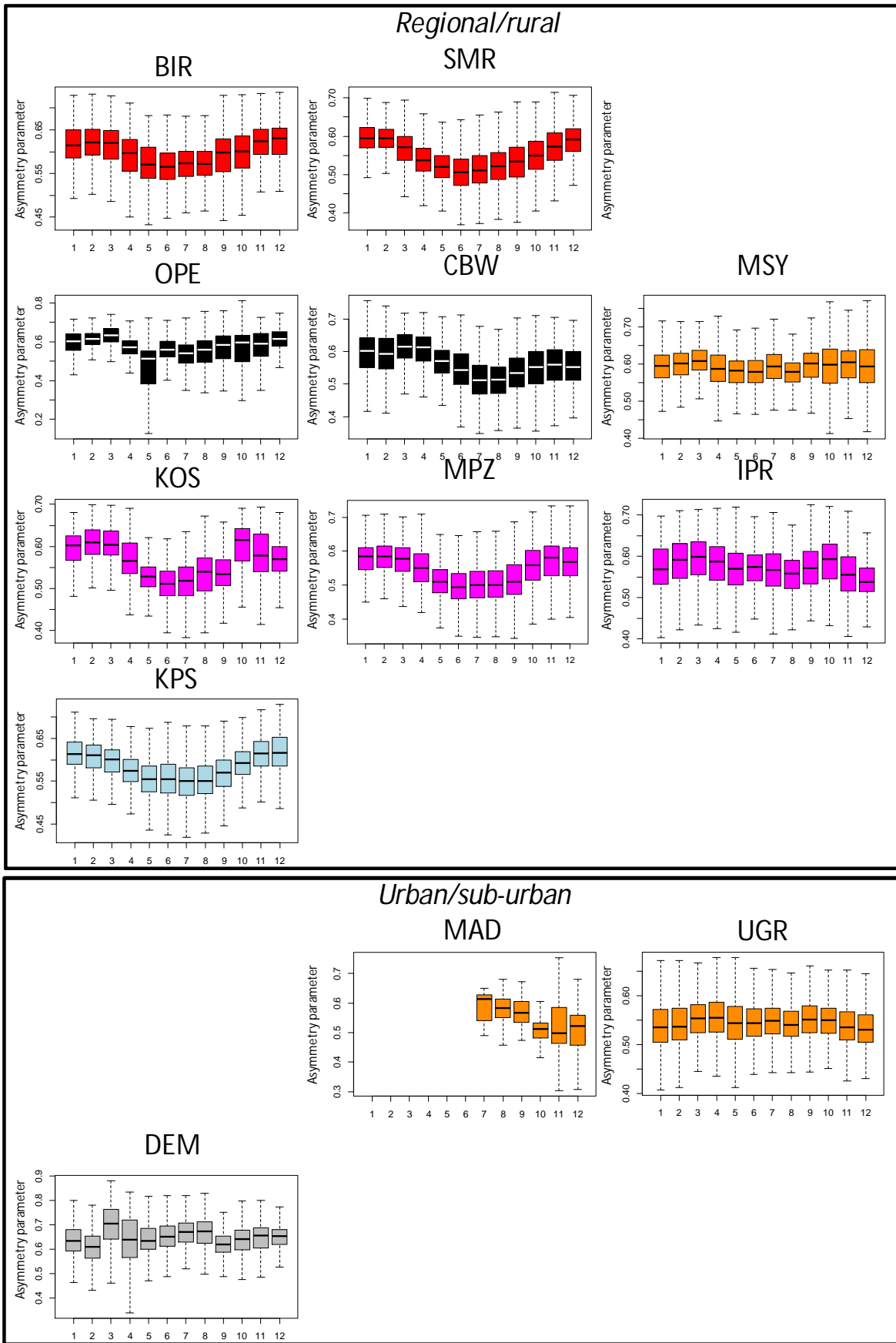
Figure 8: (Continued) Seasonal cycles of *g* (calculated for the green wavelength).
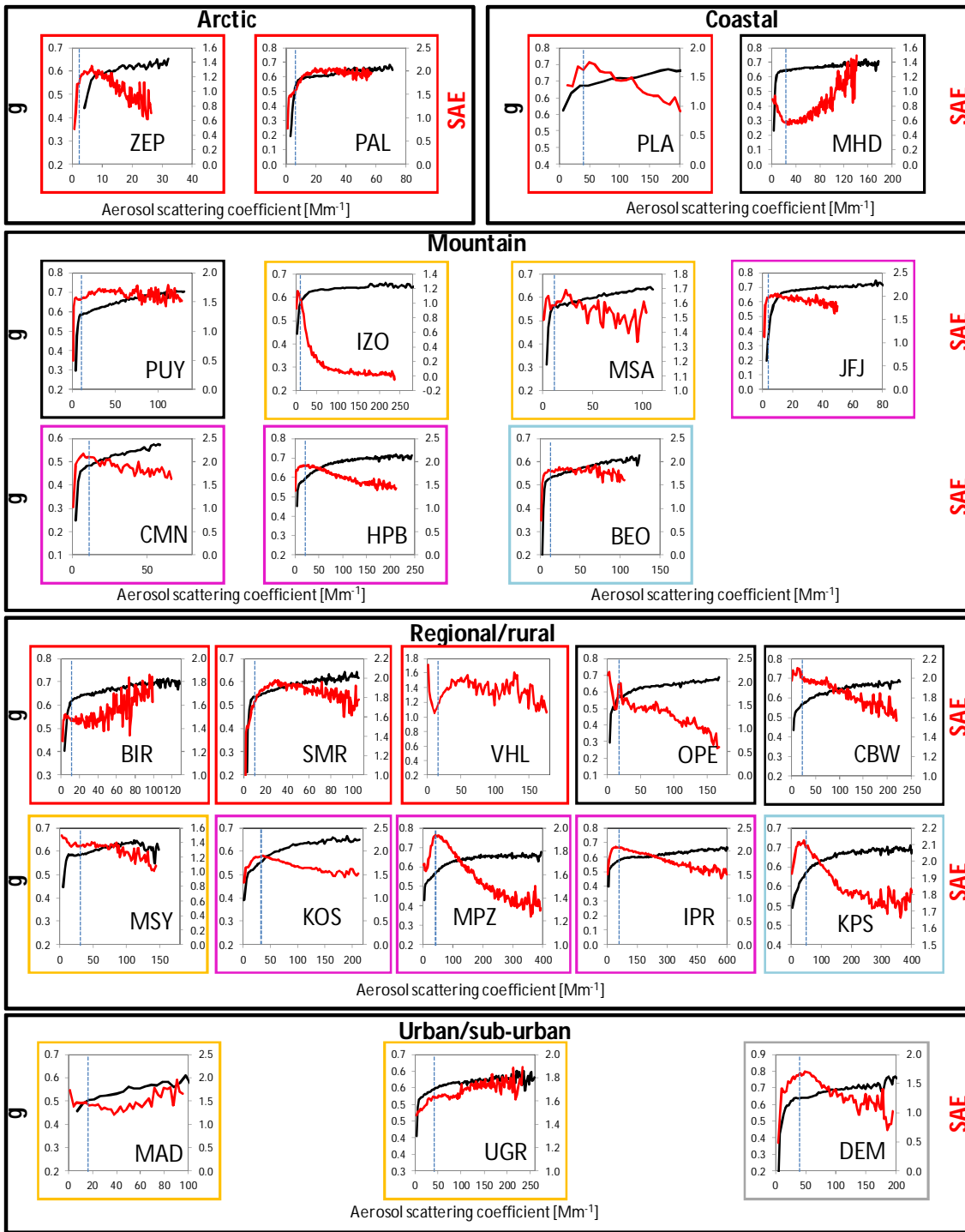
Figure 9: Scatterplots between σ_{sp} (x-axes) and SAE (right y-axes; red lines) and g (left y-axes; black lines). Dashed lines represent median σ_{sp} values at each station. Different colours highlight different geographical locations as in Figures 2, 4 and 5.